ISSN 1063-7796, Physics of Particles and Nuclei, 2010, Vol. 41, No. 1, pp. 64–100. © Pleiades Publishing, Ltd., 2010.
Original Russian Text © A.N. Sissakian, O.Yu. Shevchenko, A.P. Nagaitsev, O.N. Ivanov, 2010, published in Fizika Elementarnykh Chastits i Atomnogo Yadra, 2010, Vol. 41, No. 1.

Polarization Effects in Drell–Yan Processes

A. N. Sissakian, O. Yu. Shevchenko, A. P. Nagaitsev, and O. N. Ivanov

Abstract—Effects of polarization of hadrons and constituent quarks in Drell–Yan processes are considered; they are one of the most efficient tools for investigation of the quark structure of hadrons. Special attention is paid to such important parton distribution functions as the transversity and *T*-odd Sivers and Boer–Mulders functions whose study is necessary for understanding the effects connected with the nonzero transverse component of the quark momentum. An original method for direct extraction of transversity and Boer–Mulders function in the proton from the data on Drell–Yan processes, in which a maximum of one hadron in the initial state is transversely polarized, is presented. This method possesses a number of important advantages. The method is applied both to Drell–Yan processes with a valence antiquark (antiproton—proton and pion–proton collisions) and with a sea antiquark (proton–proton, proton–deuteron, and deuteron–deuteron collisions). Theoretical estimates of asymmetries and cross sections for setups at RHIC (BNL, US), NICA (JINR, Russia), COMPASS (CERN, Switzerland), PAX (GSI, Germany), and J-PARC (Japan) are presented for evaluation of the measurability of transversity and T-odd distributions. These theoretical estimates are accompanied by calculations of statistical uncertainties for measured asymmetries using the new Monte Carlo generator of Drell–Yan events. The duality of Drell–Yan processes and those of production of J/ψ resonance is studied, and it may allow one to considerably reduce statistical uncertainties of parton distributions. Kinematical conditions, for which this duality can be observed, are evaluated.

DOI: 10.1134/S1063779610010041

1. INTRODUCTION

From the instant of discovery of the famous spin crisis in 1987 one of the most intriguing mysteries of high-energy physics is the problem of understanding the spin structure of the nucleon. The central component of the solution of this problem, which has concentrated colossal theoretical and experimental effort for many years, is determination of polarized parton distributions in the nucleon. While at present, part of the parton's polarized distributions can be assumed rather well studied, there exist a number of important distributions which are either unknown yet or are very poorly studied, especially as it regards distributions connected with transverse polarization of the hadron and constituent partons. Finding the optimal experimental and theoretical opportunities for investigation of these "blank spots" is the objective of this paper.

In the case of zero quark transverse momenta in the leading twist approximation the quark structure of the hadron is completely described by three distribution functions (see, e.g., [1]). These are the unpolarized parton's distribution function $f_1(x) \equiv q(x)$ describing the probability of finding the parton (quark or gluon) in the hadron with the fraction x of the longitudinal momentum (independently of the parton's spin orientation); the longitudinally polarized parton's distribution function $g_1(x) \equiv \Delta q(x)$ describing the difference in the density of the number of partons with spin orientation parallel and antiparallel to the spin of the longitudinally polarized parent hadron; finally, the poorly studied transversely polarized parton's distribution function $h_1(x) \equiv \Delta T(x)$ similar to the longitudinally polarized parton's distribution function for the transversely polarized parent hadron.

On the other hand, at present of great interest are also parton distributions due to the possibility of the existence of a nonzero transverse component $\mathbf{k_T}$ of the parton momentum. The most intriguing among such distributions are two T-odd (odd with respect to time inversion) $\mathbf{k_T}$-dependent leading twist distribution functions of the parton: the Sivers function $f_{1T}^{\perp q}(x, k_T^2)$ and the Boer–Mulders function $h_{1q}^{\perp}(x, k_T^2)$. While the Sivers function represents the unpolarized parton distribution with the given $\mathbf{k_T}$ in the transversely polarized hadron, the Boer–Mulders function describes the transverse polarization of the parton with the given $\mathbf{k_T}$ in the unpolarized hadron. The Boer–Mulders function has not been measured yet, while the Sivers function [2, 3] and the transversity [4] were (preliminarily and with large uncertainties) extracted from the data of collaborations HERMES [5] and COMPASS [6] on semi-inclusive deep inelastic scattering. At the same time, the analysis of data on semi-inclusive deep inelastic scattering suffers from the poor knowledge of the fragmentation function, especially as it regards the Collins fragmentation functions necessary for measuring transversity [4]. In this relation the unique tool for investigation of parton distributions are Drell–Yan processes, since they provide direct access to a parton's distribution functions without application of any fragmentation functions. These processes (see Fig. 1.1) are characterized by the production of the lepton (electron or muon) pair in annihilation of a

quark from one colliding hadron and an antiquark from the other one. Here, it is appropriate to note that although the term "Drell–Yan processes" for reactions of this type is widely used in literature (so that we have to use it as well), it is not quite correct, since first these processes were considered in [7] by Matveev, Muradyan, and Tavkhelidze in 1969, and only a year later in [8] by Drell and Yan.

It should be underlined that along with the mentioned above important advantage (absence of fragmentation function in expressions for asymmetries and cross sections) the necessity of investigation of Drell–Yan processes is dictated by the fact that they are time-like, opposite to space-like semi-inclusive deep inelastic scattering. This is especially important for investigation of Sivers and Boer–Mulders functions: measurements of Drell–Yan processes *should* accompany measurements of processes of semi-inclusive deep inelastic scattering in order to verify the important prediction of quantum chromodynamics [9] (see also [10] and references therein):

$$f_{1T}^{\perp q}(x,k_T)\big|_{DY} = -f_{1T}^{\perp}(x,k_T)\big|_{SIDIS}, \quad (1.1)$$

$$h_1^{\perp}(x,k_T)\big|_{DY} = -h_1^{\perp}(x,k_T)\big|_{SIDIS}, \quad (1.2)$$

for the T-odd parton's distribution functions $f_{1T}^{\perp}$ and $h_1^{\perp}$. In this regard it should be noted that while the Sivers function was already extracted from the analysis of the semi-inclusive deep inelastic scattering (with poor precision, but at least with a known sign of the function $f_{1T}^{\perp}\big|_{SIDIS}$), the corresponding analysis for the function $h_1^{\perp}\big|_{SIDIS}$ has not been performed yet. Recently, in [11] the possibility of extracting azimuthal asymmetry $\langle\cos^2\phi\rangle$ (providing $h_1^{\perp}$) from the combined analysis of all existing and planned experiments on semi-inclusive deep inelastic scattering was evaluated. Thus, in the case of successful realization of this program the investigation of polarized Drell–Yan processes would allow one to verify important QCD prediction (1.1) and (1.2) for Sivers and Boer–Mulders functions.

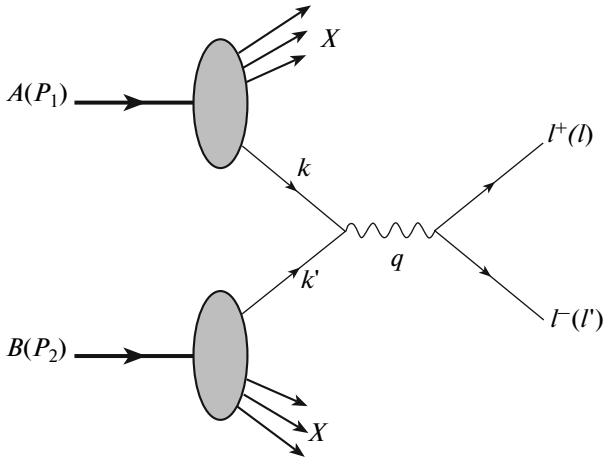

Fig. 1.1. Diagram of MMT-DY process.

2. THEORETICAL BASIS FOR INVESTIGATION OF TRANSVERSE POLARIZATION EFFECTS IN DRELL–YAN PROCESSES

The kinematic variables of the Drell–Yan process (see Fig. 1.1) are given in Table 2.1.

The process

$$H_1H_2 \longrightarrow l^+l^-X \quad (2.1)$$

Table 2.1. Kinematic variables for description of Drell–Yan process

Quantity	Description
P_1, P_2	4 momenta of hadrons
$q = Q$	4 momenta of virtual gamma quanta
$Q^2 \equiv M^2_{l^+l^-}$	squared invariant mass of the lepton pair
$s = (P_1 + P_2)^2 \simeq 2P_1P_2$	squared energy of colliding hadrons in the center of mass system
$x_1 = \frac{Q^2}{2P_1q}, \quad x_2 = \frac{Q^2}{2P_2q}$	Bjorken variables of colliding hadrons
$y = \frac{1}{2}\ln\frac{x_1}{x_2}$	rapidity
$x_F = x_1 - x_2$	Feynman variable
$x_{1,2} = \frac{\sqrt{x_F^2 + 4\tau} \pm x_F}{2} = \sqrt{\tau}e^{\pm y}$	relation between $x_{1,2}$, x_F and y

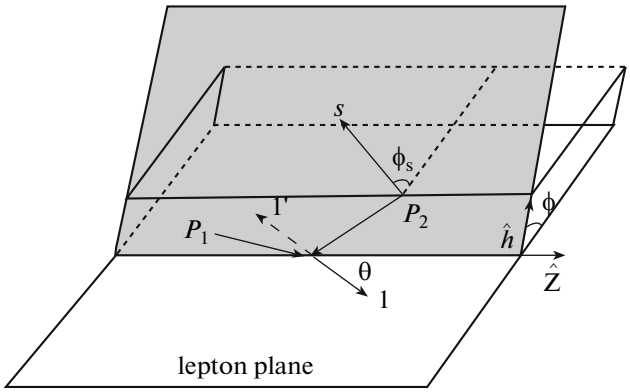

Fig. 2.1. Definition of angles in Collins–Soper reference frame.

with unpolarized hadrons in the initial state is characterized by two angles given in the center of mass system of the lepton pair (Collins–Soper system).[1] These are the polar θ and the azimuthal ϕ angles of the lepton pair shown in Fig. 2.1.

If one of the hadrons (for example, hadron H_2) in the initial state is transversely polarized, i.e., we consider the process

$$H_1 H_2^{\uparrow} \longrightarrow l^+ l^- X, \tag{2.2}$$

the additional angular variable ϕ_{S_2} determined as the azimuthal angle of the polarization vector S_2 measured with respect to the lepton plane (see Fig. 2.1) appears. In the case of Drell–Yan processes,

$$H_1^{\uparrow} H_2^{\uparrow} \longrightarrow l^+ l^- X, \tag{2.3}$$

with two polarized hadrons in the initial state, we consider two such angles ϕ_{S_1} and ϕ_{S_2}. Another measurable quantity, the transverse component of the lepton pair's momentum (see Fig. 2.2), is fundamentally important for the considered effects of the nonzero transverse component $\mathbf{k}_T$ of the quark momentum,

$$\mathbf{q}_T = \mathbf{k}_{1T} + \mathbf{k}_{1T}. \tag{2.4}$$

The probabilistic interpretation of the studied parton distributions was given above. It is reasonable to briefly consider the operator definition (see survey [1] for details).

All partons' distribution functions depending on the transverse quark momentum k_T are determined by the matrix of quark–quark correlations which have the following form in terms of the light cone's variables:

$$\Phi(x,\vec{k}_T) = \int \frac{dz^- d^2\vec{z}_T}{(2\pi)^3} \times \exp^{ipx} \langle P,S|\bar{\psi}_i(0)\mathcal{L}(0,z)\psi_i(z)|P,S\rangle, \tag{2.5}$$

where P and S are the four vectors of the hadron momentum and spin, respectively, $x = k^+/P^+$ is the Bjorken variable on the light cone, i and j are the Lorentz indices (summing is assumed over color indices) of quark operators. A special role in (2.5) is played by the gauge link

$$\mathcal{L} = \mathcal{P}\exp\left(-ig\int_0^z d\zeta^{\mu} A_{\mu}(\zeta)\right), \tag{2.6}$$

which is introduced into the bilocal operator of quark fields $\bar{\psi}(0)\psi(z)$ for preserving its gauge invariance. The k_T-dependent leading twist's distribution functions

$$[f_1(x,k_T^2), g_1(x,k_T^2), h_1(x,k_T^2)],\ [h_1^{\perp}(x,k_T^2), f_{1T}^{\perp}(x,k_T^2)]$$
$$[g_{1T}^{\perp}(x,k_T^2), h_{1L}^{\perp}(x,k_T^2)],\ h_{1T}^{\perp}(x,k_T^2)$$

are expressed in terms of correlator (2.5) as

$$\frac{1}{2}\mathrm{tr}[\gamma^+ \phi(x,\vec{k}_T)] = f_1 - \frac{\varepsilon^{jl} k_T^j S_T^l}{M_H} f_{1T}^{\perp}(x,k_T^2), \tag{2.7}$$

$$\frac{1}{2}\mathrm{tr}[\gamma^+\gamma_5 \phi(x,\vec{k}_T)] = S_L g_1(x,k_T^2) + \frac{\vec{k}_T \vec{S}_T}{M_H} g_{1T}^{\perp}(x,k_T^2), \tag{2.8}$$

$$\frac{1}{2}\mathrm{tr}[i\sigma^{j+}\gamma \phi(x,\vec{k}_T)] = S_T^j h_1 + \frac{\varepsilon^{jl} k_T^l}{M_H} h_1^{\perp}(x,k_T^2) + S_L \frac{k_T^j}{M_H} h_{1L}^{\perp} + \frac{(k_T^j k_T^l) - \frac{1}{2}k_T^2 \delta^{jl} S_T^l}{M_H^2} h_{1T}^{\perp}(x,k_T^2). \tag{2.9}$$

It was already mentioned in the Introduction that at present[2] the first priority task for all planned experi-

[1] See survey [1] for details.

[2] Lately, the increased activity on investigation of parton's distribution function called "pretzelosity" can be noted [12]. We also plan to study this interesting quantity from the point of view of its experimental observability in near future.

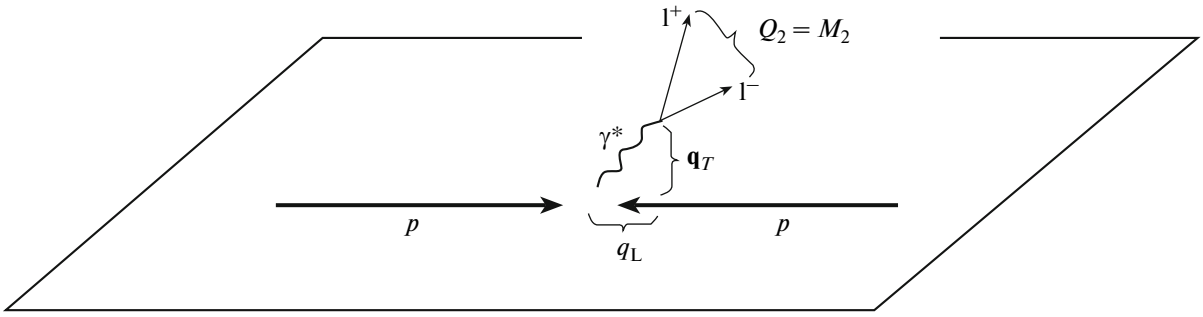

Fig. 2.2. Definition of vector $\mathbf{q}_T$.

ments concerning Drell–Yan processes is to find the transversities h_1 and T-odd Boer–Mulders $h_1^\perp$ and Sivers $f_{1T}^\perp$ distributions; the latter will be the subject of this paper.

It is well known that the investigation of Drell–Yan processes (2.3), in which both hadrons are transversely polarized in the initial state, yields the direct access to the quark and antiquark transversity's distribution functions, since they are involved in the expression for the double-spin asymmetry

$$A_{TT} = \frac{d\sigma(\vec{S}_{1\perp},\vec{S}_{2\perp}) - d\sigma(\vec{S}_{1\perp},-\vec{S}_{2\perp})}{d\sigma(\vec{S}_{1\perp},\vec{S}_{2\perp}) + d\sigma(\vec{S}_{1\perp},-\vec{S}_{2\perp})}, \qquad (2.10)$$

which in leading order QCD has the form (see survey [1] for details)

$$A_{TT} = \left|\vec{S}_{1\perp}\right|\left|\vec{S}_{2\perp}\right|\frac{\sin^2\theta\cos(2\phi-\phi_{S_1}-\phi_{S_2})}{1+\cos^2\theta} \times \frac{\sum_q e_q^2[h_{1q}(x_1,Q^2)\big|_{H_1} h_{1\bar{q}}(x_2,Q^2)\big|_{H_2} + (q\leftrightarrow\bar{q})]}{\sum_q e_q^2[f_{1q}(x_1,Q^2)\big|_{H_1} f_{1\bar{q}}(x_2,Q^2)\big|_{H_2} + (q\leftrightarrow\bar{q})]}. \qquad (2.11)$$

However, in spite of the attractiveness of double-spin asymmetries they possess an important disadvantage which often complicates their practical application. Namely, for the same number of detected Drell–Yan events double-spin asymmetries are characterized by much higher statistical errors (product of beam and target–beam polarizations in the denominator of the error expression), as compared with the single-spin asymmetries. This is especially important for Drell–Yan processes in pp (as well as pD and DD) collisions where due to small values of sea transversely polarized distribution functions of a patron predicted by QCD evolution (see, e.g., [1]) the expected values of double-spin asymmetries are also very small. This is of course important for antiproton–proton collisions in which the creation of high level polarization of the antiproton beam is at present an extremely complex and expensive task. Besides, double-spin asymmetries are fundamentally impossible for Drell–Yan processes with the pion in the initial state—it is these processes that are planned to be studied by the COMPASS collaboration in the near future. Thus, the alternative method for extraction of a transversely polarized parton's distribution functions that would allow one to avoid using polarization of both colliding hadrons is necessary. This method was developed in a number of papers [13, 14]; there, the combined analysis of unpolarized (2.1) and singly polarized (2.2) Drell–Yan processes was performed for extraction of transversity. It is also very important that processes (2.1) and (2.2) provide T-odd Boer–Mulders and Sivers functions, and the importance of investigation of these functions was discussed above.

Let us begin the consideration of processes (2.1) and (2.2) with results presented in [15] for corresponding differential cross sections obtained in the framework of the quark–parton model under the assumption of a nonzero quark's transverse momentum. We consider the case of purely transverse polarization of hadron H_2, so that it is assumed that $\lambda_1 = 0$ and $|\mathbf{S}_{1T}| = 1$ ($\lambda_2 = 0$ and $|\mathbf{S}_{2T}| = 1$ in our notation) in corresponding formulas (21) and (22) in [15]. Taking into account only dominant electromagnetic contributions (i.e., neglecting the contributions of Z_0 boson) and neglecting (similar to [15]) the contribution of higher harmonics containing the 3ϕ dependence, we obtain the following simplified formulas for the cross sections of unpolarized and singly polarized processes (2.1) and (2.2),

$$\frac{d\sigma^{(0)}(H_1H_2\to l\bar{l}X)}{d\Omega dx_1 dx_2 d^2\mathbf{q}_T} = \frac{\alpha^2}{12Q^2}\sum_q e_q^2\Big\{(1+\cos^2\theta) \times \mathcal{F}[f_{1q},f_{1q}] + \sin^2\theta\cos(2\phi) \times \mathcal{F}\left[(2\hat{\mathbf{h}}\cdot\mathbf{k}_{1T}\hat{\mathbf{h}}\cdot\mathbf{k}_{2T} - \mathbf{k}_{1T}\cdot\mathbf{k}_{2T})\frac{\bar{h}_{1q}^\perp h_{1q}^\perp}{M_1M_2}\right]\Big\}, \qquad (2.12)$$

and

$$\frac{d\sigma^{(1)}(H_1H_2^{\uparrow}\to l\dot{l}X)}{d\Omega d\phi_{S_2}dx_1dx_2d^2\mathbf{q}_T}=\frac{\alpha^2}{12Q^2}\sum_q e_q^2\Big\{(1+\cos^2\theta)\times\mathcal{F}[\dot{f}_{1q},f_{1q}]+\sin^2\theta\cos(2\phi)\times\mathcal{F}\Big[(2\hat{\mathbf{h}}\cdot\mathbf{k}_{1T}\hat{\mathbf{h}}\cdot\mathbf{k}_{2T}-\mathbf{k}_{1T}\cdot\mathbf{k}_{2T})\frac{\bar{h}_{1q}^{\perp}h_{1q}^{\perp}}{M_1M_2}\Big]+(1+\cos^2\theta)\sin(\phi-\phi_{S_2})\mathcal{F}\Big[\hat{\mathbf{h}}\cdot\mathbf{k}_{1T}\frac{\bar{f}_1^q f_{1T}^{\perp q}}{M_2}\Big]-\sin^2\theta\sin(\phi+\phi_{S_2})\mathcal{F}\Big[\hat{\mathbf{h}}\cdot\mathbf{k}_{1T}\frac{\bar{h}_{1q}^{\perp}h_{1q}}{M_1}\Big]\Big\}. \tag{2.13}$$

Here, $\hat{\mathbf{h}}\equiv\mathbf{q}_T/|\mathbf{q}_T|$, $h_{1q}(x,\mathbf{k}_T^2)$ is the k_T-dependent transversity distribution, while $h_{1q}^{\perp}(x,\ \mathbf{k}_T^2)$ and $f_{1T}^{\perp q}(x,\ \mathbf{k}_T^2)$ are the k_T-dependent T-odd (naive) Boer–Mulders and Sivers functions, respectively. The convolution products of k_T-dependent distributions included in (2.12) and (2.13) are determined as [15]

$$\mathcal{F}[\bar{f}_q f_q]\equiv\int d^2\mathbf{k}_{1T}d^2\mathbf{k}_{2T}\delta^2(\mathbf{k}_{1T}+\mathbf{k}_{2T}-\mathbf{q}_T)\times[f_q(x_1,\mathbf{k}_{1T}^2)\bar{f}_q(x_2,\mathbf{k}_{2T}^2)+(1\leftrightarrow 2)]. \tag{2.14}$$

2.1. Unpolarized Drell–Yan Processes

Let us first consider Drell–Yan processes (2.12) with unpolarized hadrons in the initial state. It can be easily seen that formula (2.12) is very inconvenient for application due to complex q_T and k_T dependences included in (2.12) via convolutions (2.14). Thus, it seems that dealing with (2.12) one cannot avoid using (poorly justified) model assumptions on the dependence of the parton's distribution function on the quark's transverse momentum k_T similar to the model proposed in [15],

$$h_{1q}^{\perp}(x,\mathbf{k}_T^2)=\frac{\alpha_T}{\pi}c_H^q\frac{M_CM_H}{\mathbf{k}_T^2+M_C^2}e^{-\alpha_T\mathbf{k}_T^2}f_{1q}(x), \tag{2.15}$$

where $M_C=2.3$ GeV, $c_H^q=1$, $\alpha_T=1$ GeV^{-1}, and M_H is the mass of hadron H. In [15, 16] this model is used to calculate the coefficient $\kappa\equiv\nu/2$ for the $\cos2\phi$-dependent part of the ratio

$$R\equiv\frac{d\sigma^{(0)}/d\Omega}{\sigma^{(0)}}, \tag{2.16}$$

which allows one to explain[3] the anomalously strong $\cos2\phi$-dependence [17, 18] of the cross section of process (2.1). However, in [15] it was underlined that (2.15) was just a crude model that should be treated cautiously. Model (2.15) cannot help to solve the main task, to extract the Boer–Mulders function $h_1^{\perp}$ from the data on unpolarized Drell–Yan processes.

In order to avoid these problems the procedure of integration/weighting with respect to the transverse momentum of the lepton pair $\mathbf{q}_T$ similar to the corresponding weighting procedures applied in [2, 19–22] with respect to other processes and studied quantities was applied in [13]. In order to use the advantages of this procedure, in [13] it was proposed to extract from unpolarized Drell–Yan processes the specially weighted and integrated with respect to $\mathbf{q}_T$ ratio of cross sections of the form (compare with (2.16))

$$\hat{R}=\frac{\int d^2\mathbf{q}_T[|\mathbf{q}_T|^2/M_1M_2][d\sigma^{(0)}/d\Omega]}{\int d^2\mathbf{q}_T\sigma^{(0)}}, \tag{2.17}$$

parameterized as

$$\hat{R}=\frac{3}{16\pi}(\gamma(1+\cos^2\theta)+\hat{k}\cos2\phi\sin^2\theta), \tag{2.18}$$

which should be compared[4] with the parameterization (see [15, 17])

$$R=\frac{3}{16\pi}(1+\lambda\cos^2\theta+\mu\sin2\theta\cos\phi+(\nu/2)\cos2\phi\sin^2\theta)\quad(\nu\equiv2\kappa,\ \lambda\simeq1,\ \mu\simeq0). \tag{2.19}$$

Using (2.12) we obtain for the coefficient $\hat{k}$ of the $\cos2\phi$-dependent part of $\hat{R}$ the following expression:

$$\hat{k}=\int d^2\mathbf{q}_T[|\mathbf{q}_T|^2/M_1M_2]\sum_q e_q^2\times\mathcal{F}\Big[(2\hat{\mathbf{h}}\cdot\mathbf{k}_{1T}\hat{\mathbf{h}}\cdot\mathbf{k}_{2T}-\mathbf{k}_{1T}\cdot\mathbf{k}_{2T})\frac{\bar{h}_{1q}^{\perp}h_{1q}^{\perp}}{M_1M_2}\Big]\times\Big(\int d^2\mathbf{q}_T\sum_q e_q^2\mathcal{F}[\bar{f}_1f_1]\Big)^{-1}, \tag{2.20}$$

[3] Note that large values of ν cannot be explained by perturbative corrections in the leading and next to leading orders of QCD expansion, as well as the effect of higher twist corrections (see [15] and references therein.

[4] It was assumed [15] upon obtaining (2.19) that $\lambda=1$ and $\mu=0$ in the most general parameterization for R (relation (5) in [15]), which is justified both by calculations in next to leading order QCD (see references in [15]) and by experimental data (see [17, 18]).

and due to the appropriately chosen weighting function $|\mathbf{q}_T|^2/M_1M_2$ the integration with respect to $\mathbf{q}_T$ results in[5] the following simple formula for $\hat{k}$:

$$\hat{k} = 8\frac{\sum_q e_q^2(h_{1q}^{\perp(1)}(x_1)h_{1q}^{\perp(1)}(x_2) + (q \leftrightarrow \bar{q}))}{\sum_q e_q^2(f_{1q}(x_1)f_{1q}(x_2) + (q \leftrightarrow \bar{q}))}, \quad (2.21)$$

where the following standard notation [20–22] is used:

$$f_q^{(n)}(x) = \int d^2\mathbf{k}_T\left(\frac{\mathbf{k}_T^2}{2M^2}\right)^n f_q(x,\mathbf{k}_T^2) \quad (2.22)$$

for the n–th moments of the $\mathbf{k}_T$-dependent parton's distribution function $f_q(x,\ \mathbf{k}_T^2)$ in the hadron with the mass M. Thus, it can be seen that the numerator of the expression for $\hat{k}$ is factorized into the simple product of the first moments of the Boer–Mulders function $h_1^\perp$. This factorization allows one to extract the *model-free* (without any model assumptions on $\mathbf{k}_T$ dependence) quantities $h_1^\perp$ from the quantity $\hat{k}$ which should be measured in unpolarized Drell–Yan processes (2.1). This, as it will be shown below, in turn, allows one to extract the transversity h_1 from the appropriately introduced in [13] weighted with respect to angular variables and transverse momentum of the lepton pair's single-spin asymmetries measured in singly polarized Drell–Yan processes (2.2). It is very important that this extraction of transversity is *model-free*: no stage of the proposed procedure uses any model assumptions concerning the dependence on the quark transverse momentum.

2.2. Single Polarized Drell–Yan Processes

Let us consider single polarized Drell–Yan processes (2.2) and determine the following single-spin asymmetries for them,

$$A_{h(f)} = \int d\Omega d\phi_{S_2}\sin(\phi \pm \phi_{S_2})[d\sigma(\mathbf{S}_{2T}) - d\sigma(-\mathbf{S}_{2T})] \times \left(\int d\Omega d\phi_{S_2}[d\sigma(\mathbf{S}_{2T}) + d\sigma(-\mathbf{S}_{2T})]\right)^{-1}, \quad (2.23)$$

where the cross section of the process is determined by formula (2.13). It can be easily seen that in the difference of the cross sections $d\sigma(\mathbf{S}_{2T}) - d\sigma(-\mathbf{S}_{2T})$ only terms containing $\sin(\phi - \phi_{S_2})$ and $\sin(\phi + \phi_{S_2})$ survive (and are multiplied by a factor of 2). Moreover, the properly[6] chosenweights $\sin(\phi + \phi_{S_2})$ and $\sin(\phi - \phi_{S_2})$ allow one to separate the contributions containing the Boer–Mulders $h_1^\perp$ and Sivers $f_{1T}^\perp$ functions; therefore, finally we obtain

$$A_h = -\frac{1}{4}\frac{\sum_q e_q^2\mathcal{F}\left[\frac{\hat{\mathbf{h}}\cdot\mathbf{k}_{1T}}{M_1}\bar{h}_{1q}^\perp h_{1q}\right]}{\sum_q e_q^2\mathcal{F}[f_{1q}f_{1q}]}, \quad (2.24)$$

and

$$A_f = \frac{1}{2}\frac{\sum_q e_q^2\mathcal{F}\left[\frac{\hat{\mathbf{h}}\cdot\mathbf{k}_{2T}}{M_2}\bar{f}_{1q}^q f_{1T}^{\perp q}\right]}{\sum_q e_q^2\mathcal{F}[f_{1q}f_{1q}]}. \quad (2.25)$$

Asymmetries similar to A_f and their application to extraction of the Sivers function

$$f_{1T}^\perp(x,\mathbf{k}_T^2) \equiv -(M/2|\mathbf{k}_T|)\Delta_{q/H^\uparrow}^N(x,\mathbf{k}_T^2) \quad (2.26)$$

from experimental data on processes (2.2) were considered in detail in [2, 3, 23, 24], and asymmetries of the type A_h which provide access to transversities and Boer–Mulders functions were studied in [13, 14, 25].

Let us begin further consideration with the asymmetry A_h determined by formulas (2.23) and (2.24). It can be easily seen that this asymmetry is inconvenient for application due to complex q_T and k_T dependences included in (2.24) via convolution (see definition (2.14)); therefore, considering this asymmetry we cannot avoid some model assumptions on the dependence of the parton's distribution function on the quark's transverse momentum. Thus, it is reasonable to apply the procedure of q_T integration/weighting again [2, 19–22] (see also its application to processes of semi-inclusive deep inelastic scattering in [5]) and consider the following asymmetry [13] instead of (2.23):

[5] Here, the following normalization condition is used: $\int d^2\mathbf{k}_T f_{1q}(x,\mathbf{k}_T^2) = f_{1q}(x)$, see, e.g., [1]).

[6] A similar procedure of weighting with respect to angular variables was earlier applied to the analysis of semi-inclusive transversely polarized deep inelastic scattering by the HERMES collaboration [5].

$$\hat{A}_h = \frac{\int d\Omega d\phi_{S_2} \int d^2\mathbf{q}_T (|\mathbf{q}_T|/M_{H_1}) \sin(\phi + \phi_{S_2}) [d\sigma(\mathbf{S}_{2T}) - d\sigma(-\mathbf{S}_{2T})]}{\int d\Omega d\phi_{S_2} \int d^2\mathbf{q}_T [d\sigma(\mathbf{S}_{2T}) + d\sigma(-\mathbf{S}_{2T})]}, \quad (2.27)$$

for which, taking into account (2.13) and (2.22), we have

$$\hat{A} = -\frac{1}{2} \frac{\sum_q e_q^2 [\bar{h}_{1q}^{\perp(1)}(x_{H_1}) h_{1q}(x_{H_2^\uparrow}) + (q \leftrightarrow \bar{q})]}{\sum_q e_q^2 [\bar{f}_{1q}(x_{H_1}) f_{1q}(x_{H_2^\uparrow}) + (q \leftrightarrow \bar{q})]}. \quad (2.28)$$

Thus, it can be seen that the numerator of the q_T-weighted asymmetry $\hat{A}_h$ is factorized into the simple algebraic product of the quantities $\bar{h}_1^{\perp(1)}$ and h_1. This provides the remarkable possibility of extracting the transversity from the measured single-spin asymmetry $\hat{A}_h$ without any model assumptions using the value of the first moment $\bar{h}_1^{\perp(1)}$ of the Boer–Mulders function which was found from the q_T-weighted quantity $\hat{k}$ (see (2.17)–(2.21)) measured in unpolarized Drell–Yan processes.

Note that the asymmetry $\hat{A}_h$ is similar to the single-spin weighted (with the angular weight $\sin(\phi - \phi_S)$ and the same weight q_T/M) asymmetry

$$A_{UT}^{\sin(\phi-\phi_S)\frac{q_T}{M}} = \frac{\int d\Omega d\phi_{S_2} \int d^2\mathbf{q}_T (|\mathbf{q}_T|/M_{H_2}) \sin(\phi - \phi_{S_2}) [d\sigma(\mathbf{S}_{2T}) - d\sigma(-\mathbf{S}_{2T})]}{\frac{1}{2}\int d\Omega d\phi_{S_2} \int d^2\mathbf{q}_T [d\sigma(\mathbf{S}_{2T}) + d\sigma(-\mathbf{S}_{2T})]}, \quad (2.29)$$

proposed in [2] (see formulas (14), (15) in [2]) for investigation of Sivers effect in single-spin processes (2.2). For this asymmetry we again observe the factorization of the contributions (compare with (2.25))

$$A_{UT}^{\sin(\phi-\phi_S)\frac{q_T}{M}} = 2\frac{\sum_q e_q^2 [\bar{f}_{1q}(x_{H_1}) f_{1T}^{\perp(1)q}(x_{H_2^\uparrow}) + (q \leftrightarrow \bar{q})]}{\sum_q e_q^2 [\bar{f}_{1q}(x_{H_1}) f_{1q}(x_{H_2^\uparrow}) + (q \leftrightarrow \bar{q})]}, \quad (2.30)$$

where

$$f_{1T}^{\perp(1)q}(x) \equiv \int d^2\mathbf{k}_T \left(\frac{\mathbf{k}_T^2}{2M_{H_2}^2}\right) f_{1T}^{\perp q}(x, \mathbf{k}_T^2) \quad (2.31)$$

is the first moment of the Sivers function.

Note that a factor of 1/2 in the denominator (2.29) (see also (7) in [26]) was introduced in [2] (where the Sivers effect was studied in Drell–Yan processes and processes of semi-inclusive deep inelastic scattering) for matching with corresponding semi-inclusive asymmetries studied by the HERMES collaboration (see [3] and references therein). Since in this paper we also study single-spin asymmetries determined by formulas (2.29) and (2.30), it is reasonable to pass over to one scale for convenience of comparison (see, e.g., the next section) and redetermine[7] the single-spin asymmetry $\hat{A}_h$ as

$$A_{UT}^{\sin(\phi-\phi_S)\frac{q_T}{M}} \equiv 2\hat{A}_n = -\frac{\sum_q e_q^2 [\bar{h}_{1q}^{\perp(1)}(x_{H_1}) h_{1q}(x_{H_2^\uparrow}) + (q \leftrightarrow \bar{q})]}{\sum_q e_q^2 [\bar{f}_{1q}(x_{H_1}) f_{1q}(x_{H_2^\uparrow}) + (q \leftrightarrow \bar{q})]}. \quad (2.32)$$

3. DRELL–YAN PROCESSES WITH A VALENCE ANTIQUARK IN THE INITIAL STATE

3.1. Antiproton–Proton Collisions

Among many possible Drell–Yan processes, processes with valence antiquark in the initial state have the obvious advantage, namely large cross sections, as compared with Drell–Yan processes with annihilating sea antiquark. In turn, Drell–Yan processes in antiproton–proton collisions, such as

$$\bar{p}p \to l^+ l^- X, \quad (3.1)$$

$$\bar{p}p^\uparrow \to l^+ l^- X, \quad (3.2)$$

$$\bar{p}^\uparrow p^\uparrow \to l^+ l^- X, \quad (3.3)$$

occupy a special place among such dominating reactions.

These processes have an important additional advantage since for them the charge conjugation's symmetry can be applied, and this symmetry results in the remarkable reduction of the number of unknown distributions involved in the measured cross sections and asymmetries of processes (3.1)–(3.3). Indeed, due to the charge conjugation, the antiquark's distribution function in the antiproton is equal to the corresponding quark's distribution function in the proton.

[7] Of course, from the practical point of view this redetermination is not very useful, upon multiplication of the asymmetry by a number the statistical error is multiplied by the same number. However, it is often convenient to study both single-spin asymmetries in the same scale in order to estimate and compare their measurability for the same statistics of Drell–Yan events.

Thus, formulas (2.21) and (2.28) for processes (3.1) and (3.2) take the form

$$\hat{k}\big|_{\bar{p}p^{\uparrow}\to l^+l^-X} = 8\frac{\sum_q e_q^2[h_{1q}^{\perp(1)}(x_1)h_{1q}^{\perp(1)}(x_2)+\bar{h}_{1q}^{\perp(1)}(x)\bar{h}_{1q}^{\perp(1)}(x_2)]}{\sum_q e_q^2[f_{1q}(x_1)f_{1q}(x_2)+\bar{f}_{1q}(x_1)\bar{f}_{1q}(x_2)]}, \quad (3.4)$$

and

$$\hat{A}_h\big|_{\bar{p}p^{\uparrow}\to l^+l^-X} = -\frac{1}{2}\frac{\sum_q e_q^2[h_{1q}^{\perp(1)}(x_1)h_{1q}^{\perp(1)}(x_2)+\bar{h}_{1q}^{\perp(1)}(x)\bar{h}_{1q}^{\perp(1)}(x_2)]}{\sum_q e_q^2[f_{1q}(x_1)f_{1q}(x_2)+\bar{f}_{1q}(x_1)\bar{f}_{1q}(x_2)]}, \quad (3.5)$$

where all distributions are *related to the proton*.

Neglecting pairwise products of distribution functions of light sea and strange quarks in the proton, we obtain

$$\hat{k}(x_1,x_2)\big|_{\bar{p}p^{\uparrow}\to l^+l^-X} \simeq 8\frac{4h_{1u}^{\perp(1)}(x_1)h_{1u}^{\perp(1)}(x_2)+h_{1d}^{\perp(1)}(x_1)h_{1d}^{\perp(1)}(x_2)}{4f_{1u}(x_1)f_{1u}(x_2)+f_{1d}(x_1)f_{1d}(x_2)}, \quad (3.6)$$

instead of (3.4), and

$$\hat{A}_h(x_1,x_2)\big|_{\bar{p}p^{\uparrow}\to l^+l^-X} \simeq -\frac{1}{2}\frac{4h_{1u}^{\perp(1)}(x_1)h_{1u}^{\perp(1)}(x_2)+h_{1d}^{\perp(1)}(x_1)h_{1d}^{\perp(1)}(x_2)}{4f_{1u}(x_1)f_{1u}(x_2)+f_{1d}(x_1)f_{1d}(x_2)}. \quad (3.7)$$

instead of (3.5). Taking into account a charge factor of 1/4 of suppression of the contribution of d quarks and the dominance of the u quark at large values[8] of x, we finally get rid of the unnecessary variables and obtain good approximations to formulas (3.4) and (3.5) of the form

$$\hat{k}(x_1,x_2)\big|_{\bar{p}p^{\uparrow}\to l^+l^-X} \simeq 8\frac{h_{1u}^{\perp(1)}(x_1)h_{1u}^{\perp(1)}(x_2)}{f_{1u}(x_1)f_{1u}(x_2)}, \quad (3.8)$$

$$\hat{A}_h(x_1,x_2)\big|_{\bar{p}p^{\uparrow}\to l^+l^-X} \simeq -\frac{1}{2}\frac{h_{1u}^{\perp(1)}(x_1)h_{1u}^{\perp(1)}(x_2)}{f_{1u}(x_1)f_{1u}(x_2)}, \quad (3.9)$$

which include only two (according to the number of equations determined by the two measured quantities $\hat{k}$ and $\hat{A}_h$) sought distribution functions $h_{1u}^{\perp(1)}$ and h_{1u}. It can be easily seen that the set of equations (3.8) and (3.9) is simple and convenient for application. Measuring $\hat{k}$ in unpolarized Drell–Yan processes (see (2.17), (2.18)) and using (3.8) we can obtain $h_{1u}^{\perp(1)}$. Then, measuring single-spin asymmetry (2.27) (or, which is the same, (2.32)) and substituting into (3.9) the known quantity $h_{1u}^{\perp(1)}$, the transversity distribution h_{1u} can be finally found.

It should be underlined once more that the proposed method of transversity extraction allows one to avoid any model assumptions on k_T-dependence of the Boer–Mulders function $h_1^{\perp}$.

Obviously, the analysis of $\hat{k}$ and $\hat{A}_h$ for extraction of $h_{1u}^{\perp(1)}$ and $h_1^{\perp}$ is considerably simplified if Eqs. (3.8) and (3.9) are considered for similar[9] (i.e., $x_F \equiv x_1 - x_2 = 0$) values of Bjorken variables for both colliding hadrons H_1 and H_2: $x_1 = x_2 \equiv x$ (i.e., $x_F \equiv x_1 - x_2 = 0$); therefore, we obtain

$$h_{1u}^{\perp(1)}(x) = f_{1u}(x)\sqrt{\frac{\hat{k}(x,x)}{8}}, \quad (3.10)$$

and

$$h_{1u}(x) = -4\sqrt{2}\frac{\hat{A}_h(x,x)}{\sqrt{\hat{k}(x,x)}}f_{1u}(x). \quad (3.11)$$

It is very important that the value of the Feynman variable x_F near zero resulting in such a remarkable simplification of extraction of $h_1^{\perp(1)}$ and h_1 corresponds to the maximal statistics of Drell–Yan events.

In order to estimate the possibility of measurement of $h_{1u}^{\perp(1)}$ and h_{1u} in processes (3.1) and (3.2) the special Monte Carlo simulation of Drell–Yan processes for kinematic conditions of PAX [52] was performed in [13]. Proton–antiproton collisions were simulated using a PYTHIA event generator [27]. Two sets of simulated data were prepared: for the collider mode (15 GeV antiproton beam colliding with a 3.5 GeV proton beam) and for the fixed target mode (22 GeV antiproton beam colliding with an internal hydrogen target). Each of the samples contains 100000 "pure" Drell–Yan events. Note that this corresponds to statistics which is planned to be achieved by the collaboration PAX. Indeed, (see [52]), the 100000 samples for the collider mode correspond to approximately 1 year of data taking for a planned luminosity of 2×10^{30} cm^{-2} s^{-1}, while for the fixed target mode this statistic corresponds to approximately 3 months of data taking for a planned luminosity of the order of 10^{31} cm^{-2} s^{-1}.

Unfortunately, the PYTHIA generator used by us does not reproduce the nontrivial q_T and x dependences of ν involved in (2.19) that were experimentally established. Thus, in order to present reliable estimates of the possibility of measurement of the parton's distribution functions $h_{1u}^{\perp(1)}$ and h_{1u} it is necessary to include these important dependences into the simula-

[8] Large values of x is the characteristic feature of experiments in $\bar{p}p$ collisions planned at GSI, see [52].

[9] Different points $x \equiv x_1 = x_2$ corresponding to $x_F = 0$ can be reached in experiment if Q^2 varies for fixed value of $s = Q^2/x_1x_2 \equiv Q^2/\tau = Q^2/x^2$.

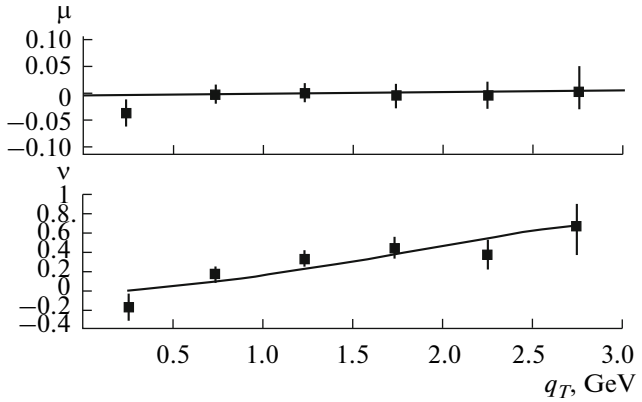

Fig. 3.1. Reconstructed dependences of the quantities μ and ν on q_T (points with error bars) from generated and weighted events in comparison with reference (corresponding to experimental data) dependences (solid lines) used in the weighting procedure.

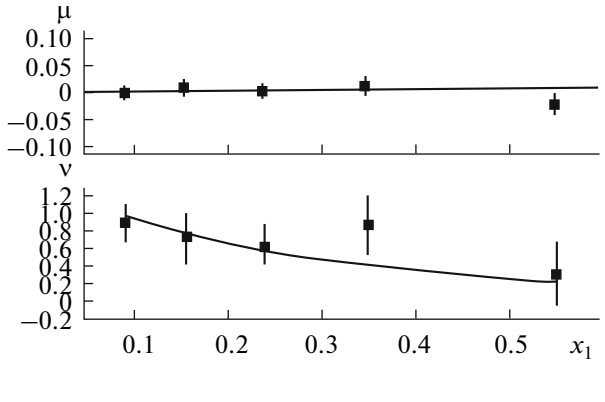

Fig. 3.2. Reconstructed dependences of the quantities μ and ν on x_1 (points with error bars) from generated and weighted events in comparison with reference (corresponding to experimental data) dependences (solid lines) used in the weighting procedure.

tion in such a way that they give the best fit to the existing experimental data. The widely used Monte Carlo method of weighting generated events was used in [13] for this purpose. In this case the weight $w = R$ is assigned to each generated event where R is given by relation (2.19) in which, according to experimental data [17, 18], $\lambda \simeq 1$, $\mu \simeq 0$, while ν nontrivially depends on q_T and x. The q_T dependence of the quantity ν is taken from [15, 16] (see (49) in [15] and (21) in [16]) and this dependence duly describes the existing experimental data [17, 18]. However, in [15, 16] (where the simplified Boer model [15] is used for $h_1^{\perp(1)}$) the x dependence of ν (which is very important and consistent with experimental data [17, 18]) is absent; therefore, this dependence is taken from [17].

In order to test the correctness of analysis of angular distributions for weighted Drell–Yan events we reconstruct q_T and x_1 dependences of ν and compare them with the corresponding template ones used in the weighting procedure obtained directly from experimental data. The results are shown in Figs. 3.1 and 3.2. Good agreement[10] between the reference values of μ and ν used in the weighting procedure and those reconstructed from the generated and weighted events can be seen from these figures.

Thus, it was proven that if the above weighting procedure is applied the results of simulation well reproduce the experimentally established nontrivial angular dependence of the ratio of cross sections R with q_T- and x- dependent coefficient ν in the $\cos 2\phi$ dependence. The successful testing allows one to apply this procedure for simulation of q_T weighted ratio of the cross sections $\hat{R}$ (see (2.17)). The corresponding results are shown in Fig. 3.3. For the averaged values of Q^2 the values of $\hat{k}$ turn out to be equal to 1.2 ± 0.2 for the collider mode and 1.0 ± 0.2 for the fixed target mode, respectively.

The quantity $h_{1u}^{\perp(1)}$ is reconstructed from the obtained values of $\hat{k}$ using (3.10) for $x_F = 0 \pm 0.04$. The results are shown in Fig. 3.4. The obtained values of $h_{1u}^{\perp(1)}$ agree (by order of magnitude) with the corresponding values obtained using the Boer model (2.15) for the Boer–Mulders function $h_{1u}^{\perp}(x, \mathbf{k}_T)$. Indeed, for example, for the collider mode ($Q^2_{average} \simeq 9$ GeV, and $x_1 \simeq x_2 \simeq 0.2$ at the point $x_F \simeq 0$) the results obtained from the simulation and from model (2.15) are $h_{1u}^{\perp(1)} \simeq 1$ and $h_{1u}^{\perp(1)} \simeq 0.5$, respectively.

Then, using the obtained values of $h_{1u}^{\perp(1)}$ we estimate the expected value of the single-spin asymmetry determined by formula (3.9). The results are shown in Figs. 3.5 and 3.6. For estimation of the transversity h_{1u} involved in the asymmetry together with $h_{1u}^{\perp(1)}$ (see (3.9)) we follow the procedure used in [28] and apply the "evolution model," in which any estimates of uncertainties are absent. That is why Figs. 5 and 6 show solid curves instead of points with error bars. In order to obtain these curves we reproduce the x-dependence of $h_{1u}^{\perp(1)}$ in the considered region using Boer model (2.15), appropriately numerically corrected according to the above simulation's results.

Evaluation of the upper boundaries of the values of h_1 and $h_1^{\perp(1)}$, and then $\hat{k}$ and $\hat{A}_h$ is very useful for a good verification of the reliability of performed esti-

[10]The used zero value of μ is reproduced as the additional verification of correctness of the applied simulation procedure.

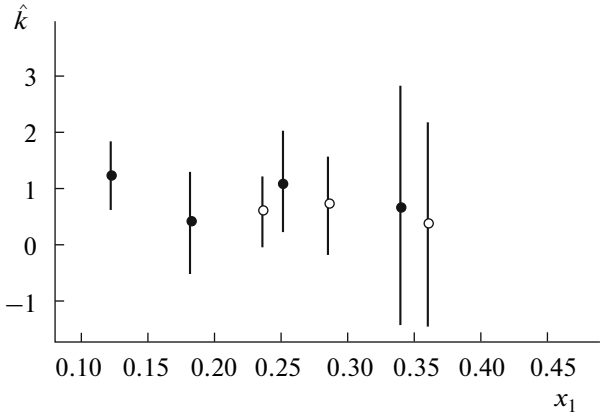

Fig. 3.3. $\hat{k}$ as a function of x_1 for $x_F \simeq 0$. Points are obtained in the Monte Carlo simulation for (dark points) collider and (open points) fixed target modes. For better perception (in order to avoid overlapping) points for the collider and fixed target modes are shifted along x by 0.01 to the left and right, respectively.

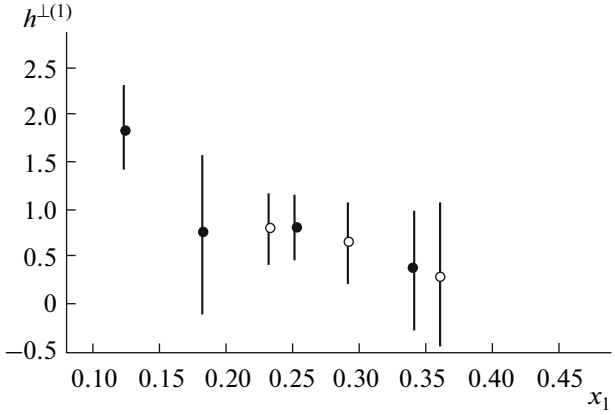

Fig. 3.4. $h_{1u}^{\perp(1)}$ as a function of x_1 for $x_F \simeq 0$. Points are obtained in Monte Carlo simulation for (dark points) collider and (open points) fixed target modes. For better perception (in order to avoid overlapping) points for the collider and fixed target modes are shifted along x by 0.01 to the left and right, respectively.

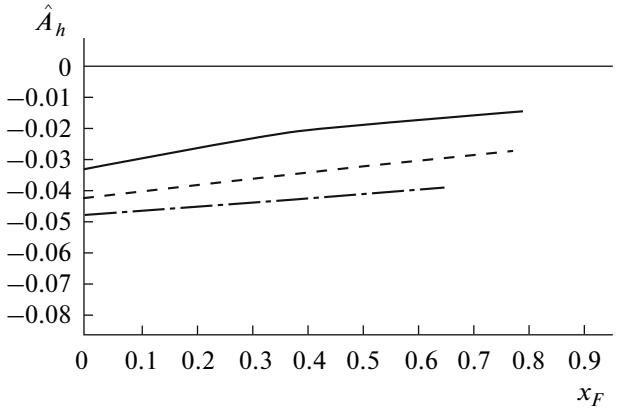

Fig. 3.5. PAX kinematics for collider mode. Single-spin asymmetry (3.9) as a function of x_F for three values of Q^2: (lower curve) 50, (intermediate curve) 25, and (upper curve) 9 GeV^2.

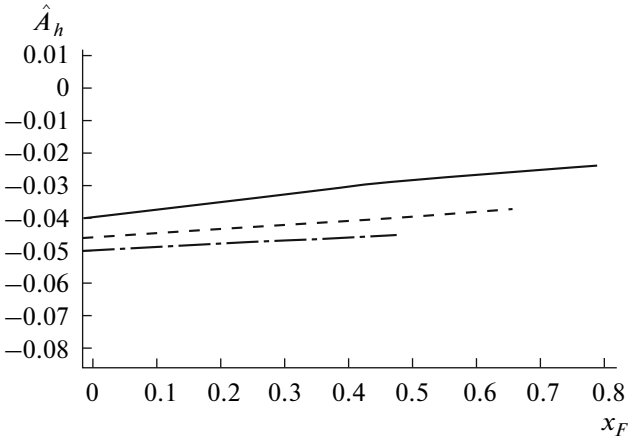

Fig. 3.6. PAX kinematics for fixed target mode. Single-spin asymmetry (3.9) as a function of x_F for three values of Q^2: (lower curve) 16, (intermediate curve) 9, and (upper curve) 4 GeV^2.

mates. Estimating $h_{1u}^{\perp(1)}$ and h_{1u}, we use formulas (3.8) and (3.9) at the points $x_1 \simeq x_2 \simeq \sqrt{Q^2/s}$; therefore, the upper boundaries for $\hat{k}$ and $\hat{A}_h$ are estimated at the points $x_F \simeq 0$ corresponding to the average value of Q^2 both for the collider and fixed target modes.

The maximal admissible value of $h_1^{\perp(1)}$ can be found similar to that done for the first moment $f_{1T}^{\perp(1)q}$ of the Sivers function in [2]. To this end we first apply the inequality

$$(|\mathbf{k}_T|/M)h_1^{\perp}(x,\mathbf{k}_T^2) \le f_1(x,\mathbf{k}_T^2),$$

which is directly obtained if constraint (16) in [29] is released (by eliminating the unknown distribution in this constraint). Then, using the estimate (see [2] and references therein)

$$\langle k_T \rangle \simeq 0.8 \text{ GeV}$$

the upper boundary for $h_{1u}^{\perp(1)}$ can be easily obtained,

$$h_{1u}^{\perp(1)} \leqslant 0.4 f_{1u}(x). \tag{3.12}$$

At the same time, the maximal admissible value of h_{1u} can be found using Soffer inequality [30],

$$|h_{1u}| \le (f_{1u} + g_{1u})/2. \tag{3.13}$$

For PAX kinematics

$$s = 43 \text{ GeV}^2,\ Q^2_{average} \simeq 5 \text{ GeV}^2,$$

for the fixed target mode, and

$$s = 215\ \text{GeV}^2,\ Q^2_{average} \simeq 9\ \text{GeV}^2,$$

for the collider mode. Thus, at the considered point $x_F = 0$ we have

$$x_1 \simeq x_2 \simeq 0.3,$$

for the fixed target mode and

$$x_1 \simeq x_2 \simeq 0.2,$$

for the collider mode. Then, constraints (3.12) and (3.13) yield[11]

$$h_{1u(max)} \simeq 1.5\ (f_{1u} = 1.9, g_{1u} = 1.0), \quad (3.14)$$

and

$$h^{\perp(1)}_{1u(max)} \simeq 0.8, \quad (3.15)$$

for the fixed target mode, and

$$h_{1u(max)} \simeq 2.3\ (f_{1u} = 3.1, g_{1u} = 1.5), \quad (3.16)$$

and

$$h^{\perp(1)}_{1u(max)} \simeq 1.2, \quad (3.17)$$

for the collider mode. Using obtained estimates (3.14)–(3.17) of the quantities $h_{1u(max)}$ and $h^{\perp(1)}_{1u(max)}$ in formulas (3.8) and (3.9), the maximal admissible values of $\hat{k}$ and $\hat{A}_h$ can be easily obtained,

$$\hat{k}_{(max)} \simeq 1.4 \quad (3.18)$$

and

$$\left|\hat{A}_{h(max)}\right| \simeq 0.17, \quad (3.19)$$

for the fixed target mode, and

$$\hat{k}_{(max)} \simeq 1.2, \quad (3.20)$$

and

$$\left|\hat{A}_{h(max)}\right| \simeq 0.14, \quad (3.21)$$

for the collider mode.

Thus, it can be seen that the obtained estimates for the upper boundaries of $h^{\perp(1)}_{1u}$, $\hat{k}$, and $\hat{A}_h$ are in good agreement with the results shown in Figs. 3.3, 3.5, and 3.6.

The estimates shown in Figs. 3.3 and 3.4 allow one to make the conclusion that for the kinematic conditions of Drell–Yan PAX experiments planned at the GSI accelerator complex the quantities $\hat{k}$ and $h^{\perp(1)}_{1u}$ are presumably measurable in most part of the x interval. At the same time, it can be seen from Figs. 3.5 and 3.6 that for both modes the single-spin asymmetry $\hat{A}_h$ is approximately estimated as 3–5%. It was argued in [52] (see Section *Single-Spin Asymmetries and Sivers Functions*) that the single-spin asymmetry $A_{UT}^{\sin(\phi-\phi_S)\frac{q_T}{M}}$ studied in [2] (see (2.29), (2.30)) of the order of 5–10% definitely can be measured by the collaboration PAX. At the same time, the asymmetry $\hat{A}_h$ weighted with $\sin(\phi+\phi_S)$ and the same weight q_T/M is similar to $A_{UT}^{\sin(\phi-\phi_S)\frac{q_T}{M}}$, except for a trivial factor of 1/2. Thus, it is obvious that if the asymmetry $A_{UT}^{\sin(\phi-\phi_S)\frac{q_T}{M}}$ of the order of 5–10% is measurable, the *similar* asymmetry $A_{UT}^{\sin(\phi-\phi_S)\frac{q_T}{M}} \equiv 2\hat{A}_h$ (see (2.32)) of order of 6–10% is also measurable, and therefore, the asymmetry $\hat{A}_h$ is measurable as well.

[11] The parameterization GRSV2000LO [31] for g_{1u} and the parameterization GRV98LO [32] for f_{1u} are used for these estimates.

3.2. Pion–Proton Collisions

Among Drell–Yan processes with a valence antiquark in the initial state the processes involving pions have an advantage. In particular, it is much easier to obtain a high intensity pion beam, as compared with an antiproton or kaon beam. Drell–Yan experiments with the pion beam, two (proton and deuteron) polarized targets, and registration of the muon pair are planned by the collaboration COMPASS [35] in the near future.

Transversity and Boer–Mulders' Distribution Functions

Let us first consider Drell–Yan processes with the negatively charged pion and unpolarized proton in the initial state,

$$\pi^- p \to \mu^+\mu^- X. \quad (3.22)$$

The general procedure [13] considered in Sections 2.1 and 2.2, as applied [25] to process (3.22), yields

$$\hat{k}\Big|_{\pi^- p \to \mu^+\mu^- X} = 8\frac{\sum_q e_q^2[\bar{h}^{\perp(1)}_{1q}(x_\pi)\big|_{\pi^-} h^{\perp(1)}_{1q}(x_p)\big|_p + (q \leftrightarrow \bar{q})]}{\sum_q e_q^2[\bar{f}_{1q}(x_\pi)\big|_{\pi^-} f_{1q}(x_p)\big|_p + (q \leftrightarrow \bar{q})]}, \quad (3.23)$$

where $\hat{k}$ is the coefficient in the $\cos 2\phi$-dependent part of the appropriately integrated over q_T ratio of the unpolarized cross sections,

$$\hat{R} = \frac{\int d^2\mathbf{q}_T[|\mathbf{q}_T|^2/M_\pi M_p][d\sigma^{(0)}/d\Omega]}{\int d^2\mathbf{q}_T \sigma^{(0)}}, \quad (3.24)$$

$$\hat{R} = \frac{3}{16\pi}(\gamma(1+\cos^2\theta) + \hat{k}\cos 2\phi \sin^2\theta). \quad (3.25)$$

At the same time, in the case of the process

$$\pi^- p^\uparrow \to \mu^+\mu^- X, \quad (3.26)$$

with the transversely polarized proton we have

(see (2.27) and (2.28))

$$\hat{A}_h = -\frac{1}{2}\frac{\sum_q e_q^2[\bar{h}_{1q}^{\perp(1)}(x_\pi)h_{1q}(x_p) + (q \leftrightarrow \bar{q})]}{\sum_q e_q^2[\bar{f}_{1q}(x_\pi)f_{1q}(x_p) + (q \leftrightarrow \bar{q})]}, \tag{3.27}$$

where the single-spin asymmetry $\hat{A}_h$ is determined as

$$\hat{A}_h = \frac{\int d\Omega d\phi_{S_2}\int d^2\mathbf{q}_T(|\mathbf{q}_T|/M_\pi)\sin(\phi-\phi_{S_2})[d\sigma(\mathbf{S}_{2T}) - d\sigma(-\mathbf{S}_{2T})]}{\frac{1}{2}\int d\Omega d\phi_{S_2}\int d^2\mathbf{q}_T[d\sigma(\mathbf{S}_{2T}) + d\sigma(-\mathbf{S}_{2T})]}. \tag{3.28}$$

Neglecting the quadratic contributions of the parton's distribution functions of strange quarks, quadratic contributions of the parton's distribution function of the sea's u quark,

$$h_{1u}^{\perp(1)}(x_\pi)\big|_{\pi^-}\bar{h}_{1u}^{\perp(1)}(x_p)\big|_p,\ h_{1u}^{\perp(1)}(x_\pi)\big|_{\pi^-}\bar{h}_{1u}(x_p)\big|_p,$$

$$f_{1u}(x_\pi)\big|_{\pi^-}\bar{f}_{1u}(x_p)\big|_p,$$

and the cross terms containing the pairwise products of the parton's distribution functions of sea and valence d quarks (additionally suppressed by a charge factor of 1/4) we obtain the following simplified equations for finding the unknown parton's distribution functions from the data

$$\hat{k}(x_\pi,x_p)\big|_{\pi^-p} \simeq 8\frac{\bar{h}_{1u}^{\perp(1)}(x_\pi)\big|_{\pi^-}h_{1u}^{\perp(1)}(x_p)\big|_p}{\bar{f}_{1u}(x_\pi)\big|_{\pi^-}f_{1u}(x_p)\big|_p}, \tag{3.29}$$

$$\hat{A}_h(x_\pi,x_p)\big|_{\pi^-p^\uparrow} \simeq -\frac{1}{2}\frac{\bar{h}_{1u}^{\perp(1)}(x_\pi)\big|_{\pi^-}h_{1u}^{\perp(1)}(x_p)\big|_{p^\uparrow}}{\bar{f}_{1u}(x_\pi)\big|_{\pi^-}f_{1u}(x_p)\big|_{p^\uparrow}}. \tag{3.30}$$

It can be easily seen that while two equations (3.8) and (3.9) corresponding to the unpolarized and singly polarized Drell–Yan processes involving antiproton–proton collisions are completely sufficient for finding the transversity and the first moment of the Boer–Mulders function in the proton, two equations (3.29) and (3.30) contain three unknown quantities $h_{1u}^{\perp(1)}(x_\pi)\big|_{\pi^-}$, $\bar{h}_{1u}^{\perp(1)}(x_p)\big|_p$, and $h_{1u}(x_p)\big|_{p^\uparrow}$. It immediately follows from Eqs. (3.29) and (3.30) that

$$\frac{h_{1u}^{\perp(1)}(x_p)\big|_p}{h_{1u}(x_p)\big|_{p^\uparrow}} = -\frac{1}{16}\frac{\hat{k}(x_\pi,x_p)\big|_{\pi^-p}}{\hat{A}_h(x_\pi,x_p)\big|_{\pi^-p^\uparrow}}. \tag{3.31}$$

Thus, using the pion beam interacting with the unpolarized and transversely polarized proton's target, the ratio of the parton's distribution functions $h_{1u}^{\perp(1)}$ and h_{1u} in the proton can be directly found. However, of course it is desirable to be able to extract the quantities $h_{1u}^{\perp(1)}(x_p)\big|_p$ and $h_{1u}\big|_{p^\uparrow}$ separately. The simplest way of solving this problem is to use the value of $h_{1u}^{\perp(1)}\big|_p$ extracted from $\hat{k}$ measured in other Drell–Yan processes (for example, in process (3.1) involving antiproton–proton collisions) in Eqs. (3.29) and (3.30). However, if one is going to extract all quantities using the pion beam (first of all, it concerns the COMPASS experiment) the additional assumptions connecting the parton's distribution functions in the pion and proton should be used. Taking into account the probabilistic interpretation of the $h_{1u}^{\perp}$ and f_{1q} (see Section 1) it is natural to assume that the following relation is satisfied:

$$\frac{\bar{h}_{1u}^{\perp(1)}(x)\big|_{\pi^-}}{\bar{h}_{1u}^{\perp(1)}(x)\big|_p} = C_u\frac{\bar{f}_{1u}(x)\big|_{\pi^-}}{f_{1u}(x)\big|_p}. \tag{3.32}$$

Note that the assumption given by relation (3.32) agrees with (but this constraint is much less stringent) the Boer model (2.15), in which

$$C_u = \frac{M_p c_\pi^u}{M_\pi c_p^u}.$$

It will be seen below that the value of C_u should be close to unity,

$$C_u \simeq 1, \tag{3.33}$$

in order to match the results for $h_{1u}^{\perp(1)}$ in the proton obtained from the simulation of $\hat{k}\big|_{\pi^-p}$ and the corresponding results obtained from the simulation of $\hat{k}\big|_{\bar{p}p}$ (see the previous section), as well as the upper boundary (see previous section) for this quantity. Thus, Eqs. (3.29) and (3.30) are rewritten in the form (compare with Eqs. (3.8) and (3.9) in the previous section)

$$\hat{k}(x_\pi,x_p)\big|_{\pi^-p} \simeq 8\frac{h_{1u}^{\perp(1)}(x_\pi)\big|_p h_{1u}^{\perp(1)}(x_p)\big|_p}{f_{1u}(x_\pi)\big|_p f_{1u}(x_p)\big|_p}, \tag{3.34}$$

$$\hat{A}_h(x_\pi,x_p)\big|_{\pi^-p^\uparrow} \simeq -\frac{1}{2}\frac{h_{1u}^{\perp(1)}(x_\pi)\big|_p h_{1u}^{\perp(1)}(x_p)\big|_p}{f_{1u}(x_\pi)\big|_p f_{1u}(x_p)\big|_p}. \tag{3.35}$$

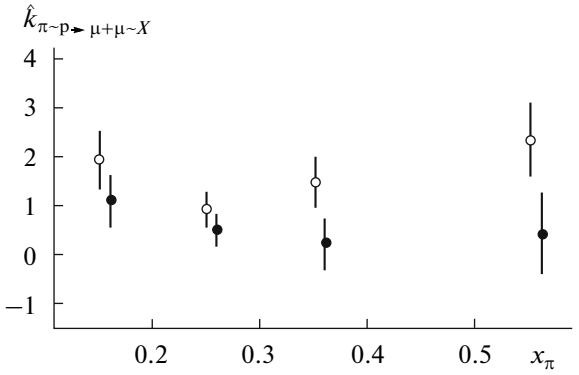

Fig. 3.7. $\hat{k}$ as a function of x_π for $x_F \simeq 0$. Data are obtained in Monte Carlo simulation for (dark points) 60 and (open points) 100 GeV pion beams.

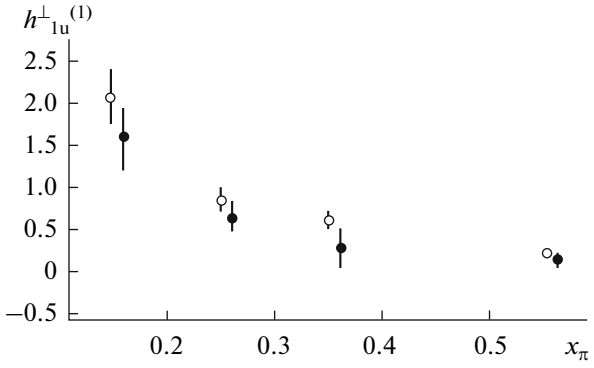

Fig. 3.8. $h_{1u}^{\perp(1)}$ as a function of x_π for $x_F \simeq 0$. Data are obtained in Monte Carlo simulation for (dark points) 60 and (open points) 100 GeV pion beams.

The following conclusion can be made from (3.34) and (3.35): now the number of equations is exactly equal to the number of sought distributions. Measuring $\hat{k}$ in an unpolarized Drell–Yan process (3.22) (see (3.24), (3.25)) and using (3.34) we can find $h_{1u}^{\perp(1)}\big|_p$. Then, measuring single-spin asymmetry (3.28) in process (3.26) and using in (3.35) the value of $h_{1u}^{\perp(1)}\big|_p$ obtained from the unpolarized Drell–Yan process, the transversity distribution $h_{1u}\big|_p$ can be ultimately found.

In practice it is more convenient to consider Eqs. (3.34) and (3.35) at the points[12] $x_\pi = x_p \equiv x$ (i.e., $x_F \equiv x_\pi - x_p = 0$), so that

$$h_{1u}^{\perp(1)}(x) = f_{1u}(x)\sqrt{\frac{\hat{k}(x,x)\big|_{\pi^-p}}{8}}, \tag{3.36}$$

and

$$h_{1u}(x) = -4\sqrt{2}\frac{\hat{A}_h(x,x)\big|_{\pi^-p^\uparrow}}{\sqrt{\hat{k}(x,x)\big|_{\pi^-p}}} f_{1u}(x), \tag{3.37}$$

where all the partons' distribution functions are *related to the proton*.

In order to evaluate the possibility of measuring $h_{1u}^{\perp(1)}$, special simulation [25] of unpolarized Drell–Yan events for COMPASS kinematics was performed. Pion–proton collisions were simulated using the PYTHIA generator [27]. Two sets of simulated data corresponding to the pion's beam energies of 60 and 100 GeV, respectively, were prepared. Each set contains about 100000 pure Drell–Yan events. Events are weighted (see the previous section) with the ratio of Drell–Yan cross sections R determined by the formula (see [15, 17])

$$R \equiv \frac{d\sigma^{(0)}/d\Omega}{\sigma^{(0)}}, \tag{3.38}$$

$$R = \frac{3}{16\pi}(1 + \cos^2\theta + (\nu/2)\cos 2\phi \sin^2\theta) \quad (\nu \equiv 2\kappa), \tag{3.39}$$

where the dependences of ν on q_T and x_π are taken from [17, 18].

The angular distributions characterizing the q_T-weighted ratio of cross sections $\hat{R}$ (see (3.24) and (3.25)) for both sets of simulated data are studied in the same way as it was done in [17] for the ratio R (see (3.38) and (3.39)). The results are shown in Fig. 3.7. The value of $\hat{k}$ for the average Q_2 corresponding to the pion's beam energies of 60 and 100 GeV turns out to be equal to 0.7 ± 0.1 and 0.9 ± 0.1, respectively.

The value of $h_{1u}^{\perp(1)}$ is reconstructed from the found values of $\hat{k}$ using (3.36) for $x_F = 0 \pm 0.04$. The results are shown in Fig. 3.8.

We recall that for obtaining $h_{1u}^{\perp(1)}$ from $\hat{k}\big|_{\pi^-p}$ it was assumed that $C_u \simeq 1$. Note that it is this value of C_u together with the results for $h_{1u}^{\perp(1)}$ obtained in the previous section from the simulated $\hat{k}\big|_{\bar{p}p}$ (compare Figs. 3.8 and 3.4) and the upper boundary for $h_{1u}^{\perp(1)}$ estimated in the previous section. In the opposite case, if the value of C_u considerably differs from unity, the values of $h_{1u}^{\perp(1)}$ presented here should be multiplied by $1/\sqrt{C_u}$, which immediately results in the mismatch of

[12] Different points $x_F = 0$ are reached by varying the value of Q^2 for the fixed value of $s \equiv Q^2/x_1x_2 \equiv Q^2/\tau$.

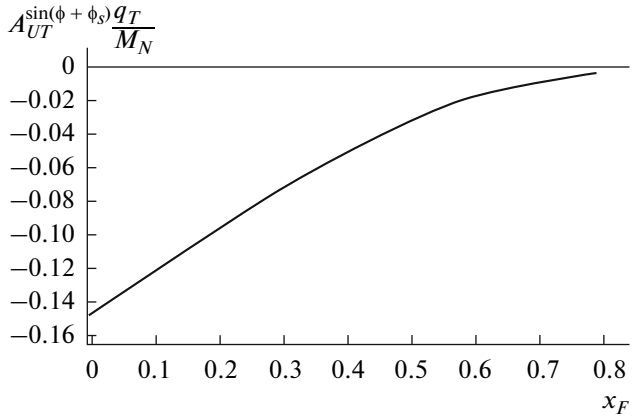

Fig. 3.9. Single-spin asymmetry (3.35) as a function of x_F for 100 GeV pion beam ($Q^2 = 6.2$ GeV^2).

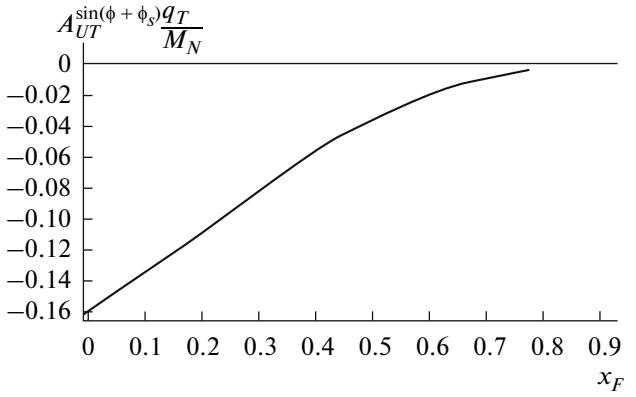

Fig. 3.10. Single-spin asymmetry (3.35) as a function of x_F for 60 GeV pion beam ($Q^2 = 5.5$ GeV^2).

the results for $h_{1u}^{\perp(1)}$ obtained from the simulated $\hat{k}\big|_{\pi^- p}$ and $\hat{k}\big|_{\bar{p}p}$.

It can be seen from Fig. 3.8 that for statistics of 100000 pure Drell–Yan events in the case of 60 GeV two points out of four are presumably observed within errors. At the same time, for a pion's beam energy of 100 GeV all four points become visible.

Of course, all conclusions made based on the Monte Carlo simulation should be considered as the preliminary ones. The final conclusion on the value of C_u can be made only based on future measurements of $\hat{k}$ in Drell–Yan processes both with the pion and the antiproton in the initial state.

Using the obtained values of $h_{1u}^{\perp(1)}$ we estimate the single-spin asymmetry determined by relations (2.32) and (3.35). The results are shown in Figs. 3.9 and 3.10. For estimating the transversity h_{1u} involved into asymmetry (2.32), (3.35) together with the first moment $h_{1u}^{\perp(1)}$ of the Boer–Mulders function we follow the procedure proposed in [28] and use the "evolution model" [1, 28], in which any estimates of uncertainties are absent. That is why Figs. 3.9 and 3.10 show solid lines instead of points with error bars. In order to obtain these curves we reproduced the x-dependence of $h_{1u}^{\perp(1)}$ in the considered region using Boer model (2.15) appropriately numerically corrected according to the results of simulation. It can be seen from Figs. 3.9 and 3.10 that the asymmetry $A_{UT}^{\sin(\phi-\phi_S)\frac{q_T}{M_N}}$ reaches a value of about 15% in the region of maximal statistics of Drell–Yan events $x_F = 0$.

It will be seen below (see Section 5) that this is sufficient for observation of the asymmetry $A_{UT}^{\sin(\phi-\phi_S)\frac{q_T}{M_N}}$ even for relatively low statistics corresponding to 50000 Drell–Yan events.

Sivers Function

In the case of processes (3.26) with a negatively charged pion and transversely polarized proton in the initial state's general expression (2.30) for the single-spin asymmetry, $A_{UT}^{\sin(\phi-\phi_S)\frac{q_T}{M_N}}\Big|_{\pi^- p^\uparrow}$ takes the form

$$A_{UT}^{\sin(\phi-\phi_S)\frac{q_T}{M_N}}\Big|_{\pi^- p^\uparrow} = 2\frac{4\hat{f}_{1u}(x_\pi)\big|_\pi f_{1T}^{\perp(1)q}(x_p)\big|_{p^\uparrow} + \hat{f}_{1d}(x_\pi)\big|_\pi f_{1T}^{\perp(1)d}(x_p)\big|_{p^\uparrow} + (q \leftrightarrow \bar{q})}{4\hat{f}_{1u}(x_\pi)\big|_\pi f_{1u}(x_p)\big|_{p^\uparrow} + \hat{f}_{1d}(x_\pi)\big|_\pi f_{1d}(x_p)\big|_{p^\uparrow} + (q \leftrightarrow \bar{q})}, \tag{3.40}$$

where negligible quadratic contributions of the s quark were omitted. Proceeding similarly to the case of the asymmetry $A_{UT}^{\sin(\phi-\phi_S)\frac{q_T}{M_N}}\Big|_{\pi^- p^\uparrow} \equiv 2\hat{A}_h$ considered above (see the procedure of obtaining (3.30)) we obtain a good approximation to (3.40) of the form

$$A_{UT}^{\sin(\phi-\phi_S)\frac{q_T}{M}}\Big|_{\pi^- p^\uparrow} \simeq 2\frac{\hat{f}_{1u}(x_\pi)\big|_\pi f_{1T}^{\perp(1)u}(x_p)\big|_{p^\uparrow}}{\hat{f}_{1u}(x_\pi)\big|_\pi f_{1u}(x_p)\big|_{p^\uparrow}}. \tag{3.41}$$

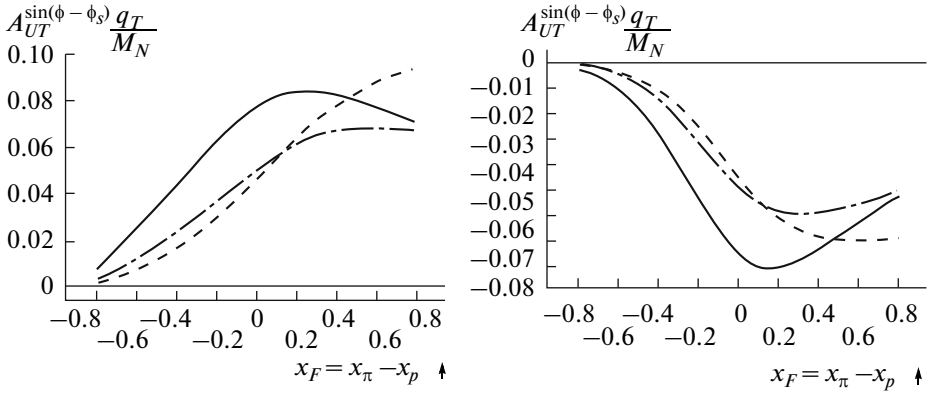

Fig. 3.11. Estimated asymmetries $A_{UT}^{\sin(\phi-\phi_S)\frac{q_T}{M}}\Big|_{\pi^- p^\uparrow}$ and $A_{UT}^{\sin(\phi-\phi_S)\frac{q_T}{M}}\Big|_{\pi^+ p^\uparrow}$ for COMPASS kinematic conditions: 160 GeV (left panel) π^- and (right panel) π^+ beams in the region $4 < Q < 9$ GeV (the corresponding average invariant mass of the lepton pair is estimated as $\langle M\rangle \simeq 5$ GeV). Solid, dashed, and dash—dotted lines correspond to fits I, II, and III (see (3.42), (3.43), (3.44)) for the Sivers function, respectively.

It can be seen that now just one unknown distribution function $f_{1T}^{\perp(1)u}(x_p)\big|_{p^\uparrow}$ unambiguously determined from the measured asymmetry $A_{UT}^{\sin(\phi-\phi_S)\frac{q_T}{M}}\Big|_{\pi^- p^\uparrow}$ is considered. It is important to underline that, as it will be demonstrated below, such an effective reduction of unnecessary variables is possible only for the π^- beam, while for the π^+ beam it is impossible to neglect most contributions into the asymmetry without risking considerably distorting the results.

Estimates for the asymmetry $A_{UT}^{\sin(\phi-\phi_S)\frac{q_T}{M}}\Big|_{\pi^- p^\uparrow}$ for the COMPASS kinematic conditions were presented in [2, 3]. Here, we repeat once more these estimates using the kinematic parameters determined more precisely (see [35]) for experiments on Drell–Yan processes planned at COMPASS. For this purpose three different fitting functions for the Sivers distributions are used in (3.40): fits I and II from [2] and the last fit from [3] denoted as fit III. These three fits are determined by the following parameterizations:

$$xf_{1T}^{\perp(1)u} = -xf_{1T}^{\perp(1)d} = 0.4x(1-x)^5, \qquad (3.42)$$

$$xf_{1T}^{\perp(1)u} = -xf_{1T}^{\perp(1)d} = 0.1x^{0.3}(1-x)^5, \qquad (3.43)$$

$$xf_{1T}^{\perp(1)u} = -xf_{1T}^{\perp(1)d} = (0.17...0.18)x^{0.66}(1-x)^5. \qquad (3.44)$$

The results of calculation of $A_{UT}^{\sin(\phi-\phi_S)\frac{q_T}{M}}\Big|_{\pi^- p^\uparrow}$ are shown in Fig. 3.11 (left panel); it can be seen from this figure that in the kinematic region available for COMPASS (the "forward" spectrometer geometry)

$$x_F = x_\pi - x_{p^\uparrow} > 0, \qquad (3.45)$$

this asymmetry assumes values of the order of 5–10%. It will be shown below (see Section 5) that these asymmetry values are sufficient for providing its measurability for COMPASS.

Beams of Negatively and Positively Charged Pions. Proton and Deuteron Targets

In the framework of the program of investigation of Drell–Yan processes, the collaboration COMPASS, first of all, plans to perform corresponding experiments with the $\pi^- p$ beam and the proton target [35]. At the same time, for solving the problem of separation of quark flavors (finding the parton's distribution functions for separate flavors) it is planned to use the $\pi^+ p$ beam [35] along with the $\pi^- p$ beam. However, it will be shown below that the availability of the $\pi^+ p$ beam does not help us to solve the flavor's separation problem, while this problem is completely solved only with the $\pi^- p$ beam if the deuteron target is used along with the proton target.

Upon finding the relation of (any) parton's distribution functions F_q in π^- (quark composition $\bar{u}d$) and π^+ (quark composition $u\bar{d}$), both the $SU_f(2)$ symmetry and the charge's conjugation symmetry C can be used simultaneously. As a result, we have

$$F_{\bar{u}}\big|_{\pi^-} \overset{C}{=} F_u\big|_{\pi^+} \overset{SU_f(2)}{=} F_d\big|_{\pi^-} \overset{C}{=} F_{\bar{d}}\big|_{\pi^+}, \qquad (3.46)$$

for valence distributions, while all sea distributions in π^- and π^+ are also equal to each other.

Taking into account (3.46) and neglecting pairwise products of a parton's distribution functions of the s quark in the pion and the proton, formula (3.23) for $\hat{k}$

takes the form

$$\hat{k}\Big|_{\pi^- p\to\mu^+\mu^- X} = 8\frac{4\bar{h}_{1u}^{\perp(1)}(x_\pi)\big|_{\pi^-}h_{1u}^{\perp(1)}(x_p)\big|_p + h_{1u}^{\perp(1)}(x_\pi)\big|_{\pi^-}h_{1d}^{\perp(1)}(x_p)\big|_p + (q\leftrightarrow\bar{q})}{4\bar{f}_{1u}(x_\pi)\big|_{\pi^-}f_{1u}(x_p)\big|_p + f_{1u}(x_\pi)\big|_{\pi^-}f_{1d}(x_p)\big|_p + (q\leftrightarrow\bar{q})}, \quad (3.47)$$

in the case of $\pi^- p$ collisions, and

$$\hat{k}\Big|_{\pi^- p\to\mu^+\mu^- X} = 8\frac{4\bar{h}_{1u}^{\perp(1)}(x_\pi)\big|_{\pi^-}h_{1d}^{\perp(1)}(x_p)\big|_p + h_{1u}^{\perp(1)}(x_\pi)\big|_{\pi^-}h_{1u}^{\perp(1)}(x_p)\big|_p + (q\leftrightarrow\bar{q})}{4\bar{f}_{1u}(x_\pi)\big|_{\pi^-}f_{1d}(x_p)\big|_p + f_{1u}(x_\pi)\big|_{\pi^-}f_{1u}(x_p)\big|_p + (q\leftrightarrow\bar{q})}, \quad (3.48)$$

in the case of $\pi^+ p$ collisions. It can be seen that in both cases only the first terms in the numerator and denominator, (3.47) and (3.48), contain the products of dominating valence distributions in the pion and proton. However, in the first case the contributions of $4h_{1u}^{\perp(1)}(x_\pi)\big|_{\pi^-}$ and $\bar{h}_{1u}^{\perp(1)}(x_p)\big|_p$ can be neglected (similar to the pairwise products of a parton's distribution functions of strange quarks), since they contain the products of two sea distributions, and the remaining cross contributions (products of the sea and valence parton's distribution functions) are additionally (noticeably) suppressed by a charge factor of 1/4 and therefore, they can also be neglected; as a result, a good approximation of (3.29) for $\hat{k}$ is obtained. In the second case, this charge suppression is absent[13], and except for the contributions

$$h_{1u}^{\perp(1)}(x_\pi)\big|_{\pi^-}\bar{h}_{1d}^{\perp(1)}(x_p)\big|_p, \quad f_{1u}(x_\pi)\big|_{\pi^-}\bar{f}_{1d}(x_p)\big|_p,$$

which contain the products of the sea parton's distribution functions we cannot neglect any term in the numerator and denominator of (3.48) without risking to considerably distort the result.

Thus, it can be seen that only the π^- beam allows one to reduce the number of unknown distribution functions of a parton to a minimum. The application of the π^+ beam in addition, although it provides one more equation, results in *two* additional unknowns at a time corresponding to the sea's Boer–Mulders distributions of the *u* quark in the pion and the proton along with the sought parton's distribution function $h_{1d}^{\perp(1)}\big|_p$ (problem of separation of *u* and *d* flavors in the proton).

Similar situation takes place for single-spin asymmetries (2.27) and (2.28) (or, which is equivalent, (2.32)) and (2.29) and (2.30). Thus, in the numerators

$$4\bar{h}_{1u}^{\perp(1)}(x_\pi)\big|_{\pi^-}h_{1u}(x_p)\big|_p + h_{1u}^{\perp(1)}(x_\pi)\big|_{\pi^-}h_{1d}(x_p)\big|_p$$
$$+ 4h_{1u}^{\perp(1)}(x_\pi)\big|_{\pi^-}\bar{h}_{1u}(x_p)\big|_p + \bar{h}_{1u}^{\perp(1)}(x_\pi)\big|_{\pi^-}\bar{h}_{1d}(x_p)\big|_p$$
$$+ (strangeness)$$

and

$$4\bar{f}_{1u}(x_\pi)\big|_{\pi^-}f_{1T}^{\perp(1)u}(x_p)\big|_p + f_{1u}(x_\pi)\big|_{\pi^-}f_{1T}^{\perp(1)d}(x_p)\big|_p$$
$$+ 4f_{1u}(x_\pi)\big|_{\pi^-}\bar{f}_{1T}^{\perp(1)u}(x_p)\big|_p + \bar{f}_{1u}(x_\pi)\big|_{\pi^-}\bar{f}_{1T}^{\perp(1)d}(x_p)\big|_p$$
$$+ (strangeness)$$

of the asymmetries $\hat{A}_h\big|_{\pi^- p^\uparrow}$ and $A_{UT}^{\sin(\phi-\phi_S)\frac{q_T}{M}}\Big|_{\pi^- p^\uparrow}$ only the first terms containing the product of two valence parton's distribution functions and a charge factor of 4 noticeably dominate. Because of it we obtain good approximations (3.30) and (3.41) for these asymmetries, reducing to a minimum the number of unknown variables. At the same time, in the numerators

$$4h_{1u}^{\perp(1)}(x_\pi)\big|_{\pi^-}h_{1u}(x_p)\big|_p + \bar{h}_{1u}^{\perp(1)}(x_\pi)\big|_{\pi^-}h_{1d}(x_p)\big|_p$$
$$+ 4\bar{h}_{1u}^{\perp(1)}(x_\pi)\big|_{\pi^-}\bar{h}_{1u}(x_p)\big|_p + h_{1u}^{\perp(1)}(x_\pi)\big|_{\pi^-}\bar{h}_{1d}(x_p)\big|_p$$
$$+ (strangeness)$$

and

$$4f_{1u}(x_\pi)\big|_{\pi^-}f_{1T}^{\perp(1)u}(x_p)\big|_p + \bar{f}_{1u}(x_\pi)\big|_{\pi^-}f_{1T}^{\perp(1)d}(x_p)\big|_p$$
$$+ 4\bar{f}_{1u}(x_\pi)\big|_{\pi^-}\bar{f}_{1T}^{\perp(1)u}(x_p)\big|_p + f_{1u}(x_\pi)\big|_{\pi^-}\bar{f}_{1T}^{\perp(1)d}(x_p)\big|_p$$
$$+ (strangeness)$$

of the asymmetries $\hat{A}_h\big|_{\pi^- p^\uparrow}$ and $A_{UT}^{\sin(\phi-\phi_S)\frac{q_T}{M}}\Big|_{\pi^- p^\uparrow}$ one can reliably neglect only the fourth terms and the strangeness contributions and leave the contributions with the unknown sea parton's distribution functions in the pion and proton. Thus, the conclusion can be made

[13] It can be seen that now the charge factor noticeably enhances two contributions in the numerator of (3.48) which contain the unknown sea parton's distribution functions $h_{1u}^{\perp(1)}\Big|_{\pi^-}$ and $\bar{h}_{1u}^{\perp(1)}\Big|_p$.

that the π^+ beam should be considered as the additional (realized in the case of a favorable situation with statistics accumulation for the π^- beam), rather than the obligatory option, which in principle may help to study sea distributions. Along with the π^- beam and the proton target it is necessary to have the deuteron target, since it allows one to solve the flavor's separation problem, i.e., find separately the parton's distribution functions for u and d quarks in the proton. Indeed, in the case of the processes

$$\pi^- D \to \mu^+ \mu^- X \tag{3.49}$$

and

$$\pi^- D^\uparrow \to \mu^+ \mu^- X, \tag{3.50}$$

applying the $SU_f(2)$ symmetry to the quark distribution functions in the proton, good approximations for $\hat{k}$, $\hat{A}_h$, and $A_{UT}^{\sin(\phi-\phi_S)\frac{q_T}{M}}$ of the following form can be easily obtained:

$$\hat{k}(x_\pi, x_D)\big|_{\pi^- D} \simeq 8\frac{\bar{h}_{1u}^{\perp(1)}(x_\pi)\big|_{\pi^-}[h_{1u}^{\perp(1)}(x_D)\big|_p + h_{1d}^{\perp(1)}(x_D)\big|_p]}{\bar{f}_{1u}(x_\pi)\big|_{\pi^-}[f_{1u}(x_D)\big|_p + f_{1d}(x_D)\big|_p]}, \tag{3.51}$$

$$A_{UT}^{\sin(\phi-\phi_S)\frac{q_T}{M}}(x_\pi, x_D)\big|_{\pi^- D^\uparrow} \equiv 2A_h(x_\pi, x_D)\big|_{\pi^- D^\uparrow} \simeq -\frac{\bar{h}_{1u}^{\perp(1)}(x_\pi)\big|_{\pi^-}[h_{1u}(x_D)\big|_p + h_{1d}(x_D)\big|_p]}{\bar{f}_{1u}(x_\pi)\big|_{\pi^-}[f_{1u}(x_D)\big|_p + f_{1u}(x_D)\big|_p]}, \tag{3.52}$$

$$A_{UT}^{\sin(\phi-\phi_S)\frac{q_T}{M}}(x_\pi, x_D)\big|_{\pi^- D^\uparrow} \simeq 2\frac{\bar{f}_{1u}(x_\pi)\big|_{\pi^-}[f_{1T}^{\perp(1)u}(x_D)\big|_p + f_{1T}^{\perp(1)d}(x_D)\big|_p]}{\bar{f}_{1u}(x_\pi)\big|_{\pi^-}[f_{1u}(x_D)\big|_p + f_{1d}(x_D)\big|_p]}; \tag{3.53}$$

These approximations together with formulas (3.29), (3.30), and (3.41) allow one to find the parton's distribution functions $h_1^{\perp(1)}$, h_1, and $f_{1T}^{\perp(1)}$ in the proton for u and d flavors.

4. DRELL–YAN PROCESSES WITH SEA ANTIQUARK IN THE INITIAL STATE

In spite of the importance of Drell–Yan processes with the annihilating valence antiquark considered above, processes with the sea antiquark in the initial state are also very important, since along with the access to valence distributions they provide access to the sea quark's distribution functions in the proton. At present, it is planned to study Drell–Yan processes in collisions of polarized protons and deuterons at the following accelerator facilities: RHIC [33] and J-PARC [34]; in principle, this option is studied as part of the Drell–Yan program[14] at COMPASS where the unpolarized proton beam and polarized proton on deuteron targets are available. The project of the new collider NICA [37, 38], based on the reconstruction of the operating accelerator Nuclotron, has started at JINR recently. It is proposed to study the properties of the quark–gluon matter in heavy ion collisions at the point of the first collision of beams of the new collider; and the investigation of the quark structure of nucleon in collisions of polarized protons and deuterons is planned to be studied at the point of the second beam's collision (see [36]). The important part of this program is the investigation of Drell–Yan processes for finding poorly known parton distribution functions in the proton. It is important to note that all these planned experiments on Drell–Yan processes do not repeat each other, but are complementary and provide different parton distribution functions[15] in different kinematic regions.

At first glance it seems that Drell–Yan processes in pp, pD, and DD collisions are strongly suppressed due to the absence of the valence antiquark in the initial state. However, it will be shown below that there exist kinematic regions in which the studied asymmetries assume rather large values to be measurable in the conditions of realistic statistics of Drell–Yan events.

4.1. Proton–Proton Collisions

Let us first consider Drell–Yan processes with unpolarized protons in the initial state,

$$pp \longrightarrow l^+ l^- X. \tag{4.1}$$

The general procedure [13] considered in Sections 2.1 and 2.2, as applied to process (4.1), yields

$$\hat{k}\big|_{pp\to l^+l^-X} = 8\frac{\sum_q e_q^2[\bar{h}_{1q}^{\perp(1)}(x_1)h_{1q}^{\perp(1)}(x_2) + (q \leftrightarrow \bar{q})]}{\sum_q e_q^2[\bar{f}_{1q}(x_1)f_{1q}(x_2) + (q \leftrightarrow \bar{q})]}, \tag{4.2}$$

[14] At present this program is focused on the pion–proton/deuteron collisions (see, e.g., [35]). However, the possibility of investigation of Drell–Yan processes in pp and pD collisions is also actively discussed by the collaboration COMPASS.

[15] For pp collisions the value of $\sqrt{s}$ makes 200 GeV for RHIC. For COMPASS this quantity varies from 20 to 27 GeV (the upper boundary corresponds to the 400 GeV primary proton SPS beam). For J-PARC it is planned to reach a value of $\sqrt{s}$ of the order of 8 GeV at the first stage and of the order of 10 GeV at the second stage. For NICA the planned value of $\sqrt{s}$ is of order of 20–26 GeV.

where $\hat{k}$ is the coefficient in the cos2ϕ-dependent part of the appropriately integrated over q_T ratio of the unpolarized cross sections

$$\hat{R} = \frac{\int d^2\mathbf{q}_T[|\mathbf{q}_T|^2/M_p^2][d\sigma^{(0)}/d\Omega]}{\int d^2\mathbf{q}_T\sigma^{(0)}}, \quad (4.3)$$

$$\hat{R} = \frac{3}{16\pi}(\gamma(1+\cos^2\theta) + \hat{k}\cos 2\phi\sin^2\theta). \quad (4.4)$$

At the same time, in the case of the process

$$pp^\uparrow \longrightarrow l^+l^-X, \quad (4.5)$$

with the transverse polarization of one of the protons we obtain (see (2.32))

$$A_{UT}^{\sin(\phi-\phi_S)\frac{q_T}{M}} \equiv 2\hat{A}_h = -\frac{\sum_q e_q^2[\bar{h}_{1q}^{\perp(1)}(x_p)h_{1q}(x_{p^\uparrow}) + (q\leftrightarrow\bar{q})]}{\sum_q e_q^2[\bar{f}_{1q}(x_p)f_{1q}(x_{p\uparrow}) + (q\leftrightarrow\bar{q})]}, \quad (4.6)$$

for the single-spin asymmetry (3.37) which provides access to the transversity and the first moment of the Boer–Mulders function, and

$$A_{UT}^{\sin(\phi-\phi_S)\frac{q_T}{M}} = 2\frac{\sum_q e_q^2[\bar{f}_{1q}(x_p)f_{1T}^{\perp(1)q}(x_{p^\uparrow}) + (q\leftrightarrow\bar{q})]}{\sum_q e_q^2[\bar{f}_{1q}(x_p)f_{1q}(x_{p^\uparrow}) + (q\leftrightarrow\bar{q})]}, \quad (4.7)$$

for asymmetry (2.29) which provides access to the first moment of the Sivers function.

Now let us consider the single-spin asymmetries determined by formulas (4.7) and (4.6). Opposite to a valence parton's distribution functions, sea distribution functions dominate for small x and decay rapidly with increasing x. That is why in the considered case of $pp^\uparrow$ collisions, the regions in which the Bjorken variable x assumes small values for sea parton's distribution functions, are most important since in this case, due to the relation

$$x_p x_{p^\uparrow} = Q^2/s, \quad (4.8)$$

a valence parton's distribution functions are found for large values of x. Indeed, in these regions the contributions into the asymmetries containing a sea parton's distribution functions for large x can be neglected (it will be seen below that this is indeed a good approximation) and due to it the number of unnecessary variables involved in the expressions for the asymmetries can be considerably reduced.

Thus, let us consider two limiting cases $x_p \gg x_{p^\uparrow}$ and $x_p \ll x_{p^\uparrow}$. In the first case

$$x_{unpol} \gg x_{pol}, \quad (4.9)$$

neglecting[16] the contributions containing a sea parton's distribution functions for large values of x_p (and correspondingly, valence ones for small values of x_p) we obtain the approximate expressions for asymmetries (4.7) and (4.6),

$$A_{UT}^{\sin(\phi-\phi_S)\frac{q_T}{M}}\Big|_{x_p\gg x_{p^\uparrow}} \simeq 2\frac{\bar{f}_{1T}^{\perp(1)u}(x_{p^\uparrow})f_{1u}(x_p) + \bar{f}_{1T}^{\perp(1)d}(x_{p^\uparrow})f_{1d}(x_p)}{4\bar{f}_{1u}(x_p)\bar{f}_{1u}(x_{p^\uparrow}) + f_{1d}(x_{p^\uparrow})f_{1d}(x_p)}, \quad (4.10)$$

and

$$A_{UT}^{\sin(\phi-\phi_S)\frac{q_T}{M}}\Big|_{x_p\gg x_{p^\uparrow}} \simeq -\frac{4h_{1u}^{\perp(1)}(x_p)\bar{h}_{1u}(x_{p^\uparrow}) + h_{1d}^{\perp(1)}(x_p)\bar{h}_{1d}(x_{p^\uparrow})}{4f_{1u}(x_p)\bar{f}_{1u}(x_{p^\uparrow}) + f_{1d}(x_p)\bar{f}_{1d}(x_{p^\uparrow})}. \quad (4.11)$$

Then, taking into account quark charges and the u quark's dominance at large x, relations (4.10) and (4.11) are reduced to the simplified equations

$$A_{UT}^{\sin(\phi-\phi_S)\frac{q_T}{M}}\Big|_{x_p\gg x_{p^\uparrow}} \simeq 2\frac{\bar{f}_{1T}^{\perp(1)u}(x_{p^\uparrow})f_{1u}(x_p)}{\bar{f}_{1u}(x_{p^\uparrow})f_{1u}(x_p)} = 2\frac{\bar{f}_{1T}^{\perp(1)u}(x_{p^\uparrow})}{\bar{f}_{1u}(x_{p^\uparrow})}, \quad (4.12)$$

and

$$A_{UT}^{\sin(\phi-\phi_S)\frac{q_T}{M}}\Big|_{x_p\gg x_{p^\uparrow}} \simeq -\frac{h_{1u}^{\perp(1)}(x_p)\bar{h}_{1u}(x_{p^\uparrow})}{f_{1u}(x_p)\bar{f}_{1u}(x_{p^\uparrow})}, \quad (4.13)$$

which will be shown below to be good approximations to the considered symmetries.

Acting in a similar way, in the second limiting case

$$x_{unpol} \ll x_{pol}, \quad (4.14)$$

we obtain

$$A_{UT}^{\sin(\phi-\phi_S)\frac{q_T}{M}}\Big|_{x_p\ll x_{p^\uparrow}} \simeq 2\frac{f_{1T}^{\perp(1)u}(x_{p^\uparrow})\bar{f}_{1u}(x_p) + f_{1T}^{\perp(1)d}(x_{p^\uparrow})\bar{f}_{1d}(x_p)}{4f_{1u}(x_p)\bar{f}_{1u}(x_{p^\uparrow}) + f_{1d}(x_{p^\uparrow})\bar{f}_{1d}(x_p)}, \quad (4.15)$$

and

$$A_{UT}^{\sin(\phi-\phi_S)\frac{q_T}{M}}\Big|_{x_p\ll x_{p^\uparrow}} \simeq -\frac{4\bar{h}_{1u}^{\perp(1)}(x_p)h_{1u}(x_{p^\uparrow}) + \bar{h}_{1d}^{\perp(1)}(x_p)h_{1d}(x_{p^\uparrow})}{4\bar{f}_{1u}(x_p)f_{1u}(x_{p^\uparrow}) + \bar{f}_{1d}(x_p)f_{1d}(x_{p^\uparrow})}, \quad (4.16)$$

[16] Similar to the above, we eliminate the contributions of strangeness which yield very small corrections.

taking into account the contribution of the d quark; and

$$A_{UT}^{\sin(\phi-\phi_S)\frac{q_T}{M}}\Big|_{x_p \ll x_{p^\uparrow}} \simeq 2\frac{f_{1T}^{\perp(1)u}(x_{p^\uparrow})\bar{f}_{1u}(x_p)}{f_{1u}(x_{p^\uparrow})\bar{f}_{1u}(x_p)} = 2\frac{f_{1T}^{\perp(1)u}(x_{p^\uparrow})}{f_{1u}(x_{p^\uparrow})}, \tag{4.17}$$

and

$$A_{UT}^{\sin(\phi-\phi_S)\frac{q_T}{M}}\Big|_{x_p \ll x_{p^\uparrow}} \simeq -\frac{\bar{h}_{1u}^{\perp(1)}(x_p)h_{1u}(x_{p^\uparrow})}{\bar{f}_{1u}(x_p)f_{1u}(x_{p^\uparrow})}, \tag{4.18}$$

if this contribution is neglected.

It will be shown below that even double approximations determined by (4.13) and (4.18) are in a very good agreement with the original formula (4.6) for the asymmetry $A_{UT}^{\sin(\phi-\phi_S)\frac{q_T}{M}}$. It is very important, since it allows one to considerably reduce the number of unknown variables (an unknown parton's distribution functions) included in the equations determined by the asymmetry $A_{UT}^{\sin(\phi-\phi_S)\frac{q_T}{M}}$ measured in kinematic regions (4.9) and (4.14). In particular, this provides an interesting possibility of direct extraction of the ratios $h_{1u}/h_{1u}^{\perp(1)}$ and $\bar{h}_{1u}/\bar{h}_{1u}^{\perp(1)}$, i.e., finding these ratios directly from data without a fitting procedure applying a number of assumptions concerning the unknown distribution functions. Indeed, let us consider unpolarized Drell–Yan process (4.1). In the limiting cases $x_1 \gg x_2$ and $x_1 \ll x_2$, Eq. (4.2) is reduced to the equations

$$\hat{k}\big|_{x_1 \gg x_2} \simeq 8\frac{h_{1u}^{\perp(1)}(x_1)\bar{h}_{1u}^{\perp(1)}(x_2)}{f_{1u}(x_1)\bar{f}_{1u}(x_2)}, \tag{4.19}$$

and

$$\hat{k}\big|_{x_1 \ll x_2} \simeq 8\frac{\bar{h}_{1u}^{\perp(1)}(x_1)h_{1u}^{\perp(1)}(x_2)}{\bar{f}_{1u}(x_1)f_{1u}(x_2)}, \tag{4.20}$$

respectively. Then, if the quantities $\hat{k}(x_1, x_2)$ and $A_{UT}^{\sin(\phi-\phi_S)\frac{q_T}{M}}$ $(x_p = x_1, x_{p^\uparrow} = x_2)$ measured in the unpolarized and single polarized Drell–Yan processes are known, combining (4.13), (4.18) and (4.19), (4.20), the ratios $h_{1u}/h_{1u}^{\perp(1)}$ and $\bar{h}_{1u}/\bar{h}_{1u}^{\perp(1)}$ can be obtained from the equations

$$\frac{\bar{h}_{1u}(x_1)}{\bar{h}_{1u}^{\perp(1)}(x_1)} \simeq -8\frac{\hat{A}_{UT}^{\sin(\phi-\phi_S)\frac{q_T}{M}}}{\hat{k}}\Big|_{x_p \ll x_{p^\uparrow}},$$
$$\frac{h_{1u}(x_1)}{h_{1u}^{\perp(1)}(x_1)} \simeq -8\frac{\hat{A}_{UT}^{\sin(\phi-\phi_S)\frac{q_T}{M}}}{\hat{k}}\Big|_{x_p \gg x_{p^\uparrow}}. \tag{4.21}$$

Numerical Estimates for Asymmetries

Let us present the estimates for the values of the asymmetry $A_{UT}^{\sin(\phi-\phi_S)\frac{q_T}{M}}\Big|_{pp^\uparrow \to l^+l^-X}$ determined by (4.7). Note that for RHIC kinematics the asymmetry $A_{UT}^{\sin(\phi-\phi_S)}$ weighted with the angular factor $\sin(\phi-\phi_S)$ was only just studied in [26]. In the framework of the Gaussian model applied in [26] this asymmetry is proportional to the studied q_T-weighted asymmetry $A_{UT}^{\sin(\phi-\phi_S)\frac{q_T}{M}}$,

$$A_{UT}^{\sin(\phi-\phi_S)} = a_{Gauss}^{DY}A_{UT}^{\sin(\phi-\phi_S)\frac{q_T}{M}}$$
$$a_{Gauss}^{DY} \simeq 0.81(1 \pm 10\%), \tag{4.22}$$

and it is not necessary to repeat calculations for RHIC kinematic region. Instead, we present the estimates for NICA kinematics [37, 38] where it is planned to collide 10–13 GeV proton beams. The calculations are performed for Q^2 below and above the production threshold $Q^2 = 9.5$ GeV^2 of the J/ψ resonance. Similar to the above (see Section 3.2), fits I, II, and III for the Sivers function determined by formulas (3.42)–(3.43) are used in calculations. For the first moments of the Sivers function involved in (4.7)

$$\bar{f}_{1T}^{\perp(1)q}(x) \equiv \int d^2\mathbf{k}_T\left(\frac{\mathbf{k}_T^2}{2M_p^2}\right)\bar{f}_{1T}^{\perp q}(x,\mathbf{k}_T^2),$$

we use the model (with positive sign) proposed in [26] (see (10) and (11) in [26]),

$$\frac{\bar{f}_{1T}^{\perp(1)\bar{q}}(x)}{\bar{f}_{1T}^{\perp(1)q}(x)} = \frac{f_{1\bar{u}}(x)+f_{1\bar{d}}(x)}{f_{1u}(x)+f_{1d}(x)}. \tag{4.23}$$

The parameterization GRV94 [39] is used for an unpolarized parton's distribution functions included in (4.7).

The results of calculation of $A_{UT}^{\sin(\phi-\phi_S)\frac{q_T}{M}}$ for different values of Q^2 are shown in Fig. 4.1. It can be seen from this figure that the asymmetry assumes the largest values, of the order of 6–8% near the zero value of the difference $x_p - x_{p^\uparrow}$ when this difference is positive. It

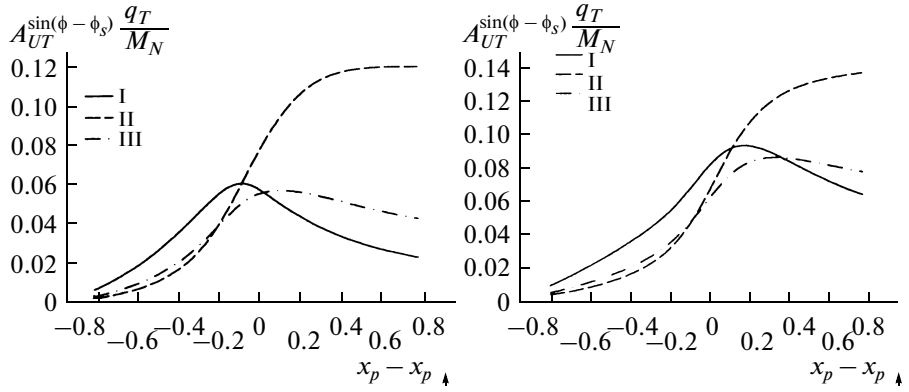

Fig. 4.1. Estimated asymmetries $A_{UT}^{\sin(\phi-\phi_S)\frac{q_T}{M}}\Big|_{pp^\uparrow}$ for NICA: $s = 400$ GeV^2, $Q^2 =$ (left panel) 4 and (right panel) 15 GeV^2. Numbers I, II denote fits I, II for the Sivers function (see [2]). Number III denotes fit from [3].

will be shown below (see Section 5) that such values of asymmetry are quite sufficient to provide its measurability in the conditions of the collider NICA.

Note that along with parameterizations I, II, and III, there exist parameterizations for the Sivers function given in [40, 41]. Our calculations[17] show that the values of $A_{UT}^{\sin(\phi-\phi_S)\frac{q_T}{M}}$ obtained using these parameterizations are very close to the corresponding values for parameterizations I, II, and III in the region $x_p > x_{p^\uparrow}$ and exceed them in the region $x_p < x_{p^\uparrow}$. Thus, the prediction for $A_{UT}^{\sin(\phi-\phi_S)\frac{q_T}{M}}$ made using parameterizations (3.42)–(3.43) can be considered as the underestimate for this asymmetry: if the asymmetry's $A_{UT}^{\sin(\phi-\phi_S)\frac{q_T}{M}}$ value calculated using parameterizations I, II, and III is sufficient for its measurability with the given statistics of Drell–Yan events, an even larger asymmetry value obtained using parameterizations from [40, 41] is all the more sufficient for measurability.

Figures for $A_{UT}^{\sin(\phi-\phi_S)\frac{q_T}{M}}$ corresponding to our calculations performed for COMPASS and J-PARC kinematic conditions (unlike RHIC conditions, they are very close to NICA kinematic conditions) are very similar to Fig. 4.1 for NICA kinematics, reproducing practically the same behavior of this asymmetry. This behavior of $A_{UT}^{\sin(\phi-\phi_S)\frac{q_T}{M}}$ allows one to hope that it can be measured not only in the collider mode (RHIC and NICA), but also in fixed target experiments (COMPASS and J-PARC). The matter is that in fixed target experiments, as a rule, the detector acceptance allows one to register mainly events with a positive Feynman variable x_F,

$$x_F \equiv x_{beat} - x_{target} \simeq 0, \tag{4.24}$$

where x_{beam} and x_{target} are the values of the Bjorken variable x for quarks in the protons of the beam and target, respectively. Thus, the option $x_p > x_{p^\uparrow}$ in principle can be realized at COMPASS and J-PARC where the unpolarized proton beam and the polarized proton target will be available. On the other hand, the region $x_p < x_{p^\uparrow}$, where $A_{UT}^{\sin(\phi-\phi_S)\frac{q_T}{M}}$ also assumes rather large values can be reached in collider experiments at RHIC and NICA, and maybe in experiments at J-PARC (where the option with the polarized proton beam is also planned, see [34]).

Let us consider the asymmetry $A_{UT}^{\sin(\phi-\phi_S)\frac{q_T}{M}}$ determined by relation (4.6). Since neither the Boer–Mulders function, nor its first moment have been measured yet, we use Boer model (2.15) in calculations; this model provides a good fit for experimental data of NA10 [18] and E615 [17] for the (anomalously large) $\cos(2\phi)$-dependence of Drell–Yan cross sections. In the framework of this model the first moment

$$h_{1q}^{\perp(1)}(x) \equiv \int d^2\mathbf{k}_T \left(\frac{\mathbf{k}_T^2}{2M^2}\right) h_{1q}^{\perp(1)}(x, \mathbf{k}_T^2)$$

[17] Considering the parameterization from [40] it should be taken into account that the notation for the Sivers function $\Delta^N f_{q/H^\uparrow}$ and $f_{1T}^\perp$ have different signs and the following factor: $f_{1T}^\perp(x, \mathbf{k}_T^2) = -(M/2|\mathbf{k}_T|)\Delta^N f_{q/H^\uparrow}(x, \mathbf{k}_T^2)$ (see "Trento conventions" in [42]).

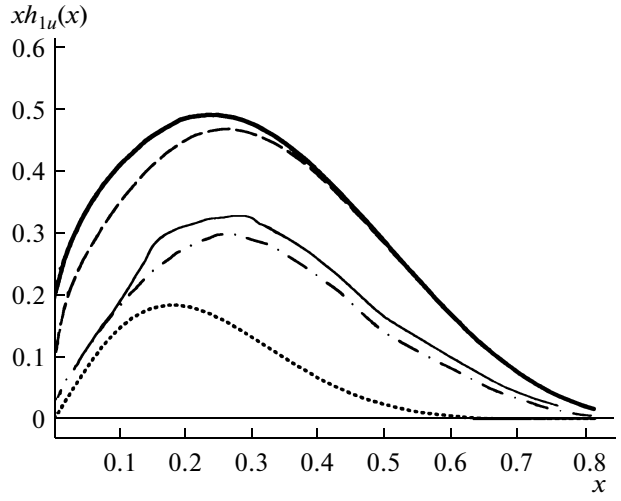

Fig. 4.2. Results from [4] for h_{1u} in comparison with results obtained using two versions of the evolution model and Soffer inequality. Continuous thick line (upper curve) corresponds to the upper boundary determined by Soffer inequality. Dashed line corresponds to the evolution model with saturation of Soffer inequality for the initial model scale $Q^2 = 0.23$ GeV^2. Continuous thin line corresponds to the upper boundary of the error band for h_{1u}. Dash–dotted line corresponds to the fitting function for h_{1u} from [4]. Parameterizations GRV94 [39] and GRSV95 [68] for $q(x)$ and $\Delta q(x)$, respectively, are used.

of the Boer–Mulders function $h_{1q}^{\perp(1)}$ assumes the value

$$h_{1q}^{\perp(1)}(x) \simeq 0.163 f_1(x).$$

We also use the following assumption for the first moment of the Boer–Mulders' distribution function of the sea quark:

$$\frac{h_{1\bar{q}}^{\perp(1)}(x)}{h_{1q}^{\perp(1)}(x)} = \frac{f_{1\bar{q}}(x)}{f_{1q}(x)}. \tag{4.25}$$

Note that this assumption looks like assumption (4.23) used above, but is not similar to it. In this case, it is the assumption in form (4.25) that is consistent with the Boer model under discussion.

The transversity parton's distribution function h_1 was first extracted [4] from the combined data of the collaborations HERMES [5], COMPASS [43], and BELLE [44]. However, due to the poor quality of these data the error band for h_1 parameterization was very large (see Fig. 4.2), and in [4] a large number of additional assumptions were used for analysis. In particular, the assumption of zero distribution functions of a parton for sea quark transversity was applied. However, it was already noted more than once that in the case of proton–proton collisions it is a sea parton's distribution functions that play the decisive role. That is why we use two versions of the evolution model for transversity instead of the transversity parameterization from [4]. The first one is the model presented in [45] where for a very small value of Q^2 ($Q_0^2 = 0.23$ GeV^2) (so called "model scale") Soffer inequality (3.13) is saturated,

$$\begin{aligned} h_{1q}(x,Q_0^2) &= \frac{1}{2}[q(x,Q_0^2) + \Delta q(x,Q_0^2)], \\ \bar{h}_{1q}(x,Q_0^2) &= \frac{1}{2}[\bar{q}(x,Q_0^2) + \Delta\bar{q}(x,Q_0^2)], \end{aligned} \tag{4.26}$$

and then the quantities h_{1q} and $h_{1\bar{q}}$ evolve according to Dokshitzer–Gribov–Lipatov–Altarelli–Parisi (DGLAP) equations. Of course, this model gives the upper boundary for the asymmetry. In the other version of the evolution model (see [1, 28]) for the same initial value of Q_0^2 (model scale), the valence and sea parton's distribution functions for transversity in the proton are assumed to be equal to the corresponding longitudinally polarized parton's distribution functions, and

$$\begin{aligned} h_{1q}(x;Q_0^2) &= \Delta q(x;Q_0^2), \\ \bar{h}_{1q}(x;Q_0^2) &= \Delta\bar{q}(x;Q_0^2), \end{aligned} \tag{4.27}$$

and then $h_{1\bar{q}}$ again evolves to the considered values of Q^2 according to DGLAP equations. Of course, this model is much more realistic, since for the initial model scale many models predict [1] the satisfaction of (4.27). It is very important that the transversity curve corresponding to this version of the evolution model is within the error band for the fit from [4] (see Fig. 4.2). Thus, the evolution model with initial conditions (4.27) is in agreement with the results of [4].

Here, we present the estimates for the asymmetry $A_{UT}^{\sin(\phi-\phi_S)\frac{q_T}{M}}$ below and above the J/ψ resonance's prduction threshold for strongly different RHIC (Fig. 4.3) and NICA (Fig. 4.4) kinematic conditions. The corresponding figures for COMPASS and J-PARC kinematics practically do not differ from Fig. 4.4, in which the results are displayed for NICA kinematic conditions.

It can be seen from Figs. 4.3 and 4.4 that for RHIC and NICA (as well as for COMPASS and J-PARC) kinematics the asymmetry $A_{UT}^{\sin(\phi-\phi_S)\frac{q_T}{M}}$ is negligible for $x_p > x_{p^\uparrow}$ and takes rather large values in the region $x_p < x_{p^\uparrow}$. In the second case, $A_{UT}^{\sin(\phi-\phi_S)\frac{q_T}{M}}$ reaches maximal values (of the order of 5–10%) when the difference $x_p - x_{p^\uparrow}$ assumes large negative values. Therefore, the conclusion can be made that the symmetric collider mode (RHIC and NICA), for which the cases $x_p < x_{p^\uparrow}$ and $x_p > x_{p^\uparrow}$ do not differ, has an advantage, as compared to the fixed target mode for which these cases considerably differ due to constraint (4.24) on the detector acceptance. Thus, in order to obtain nonzero

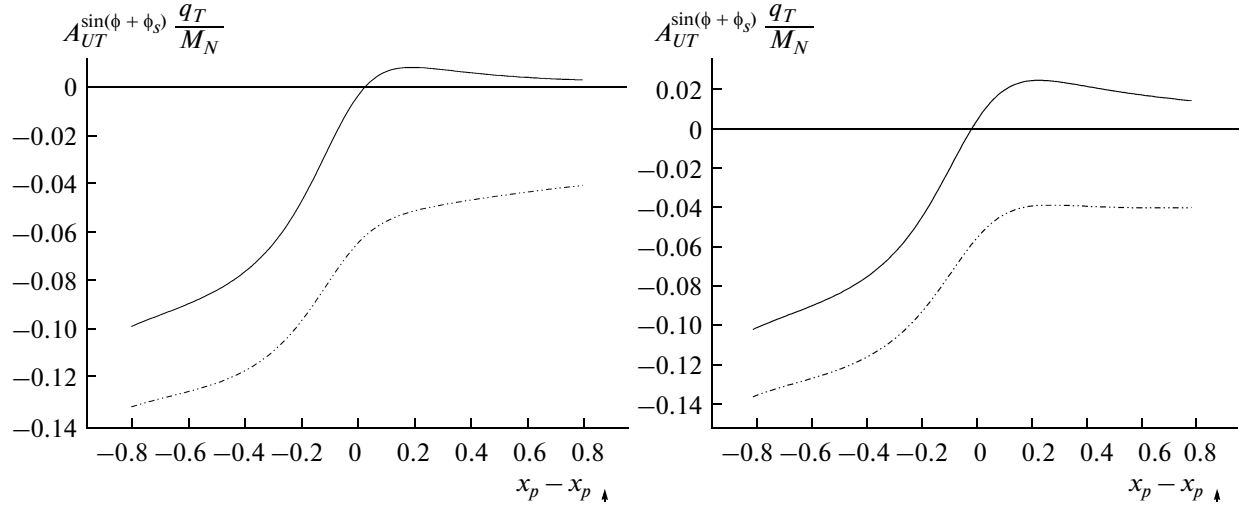

Fig. 4.3. Estimate of asymmetry $A_{UT}^{\sin(\phi+\phi_S)\frac{q_T}{M}}\Big|_{pp^\uparrow}$ for RHIC, $s = 200^2$ GeV^2 for $Q^2 =$ (left panel) 4 and (right panel) 20 GeV^2. Solid and dashed lines correspond to two versions of evolution model (4.26) and (4.27) for transversity. The parameterizations GRV94 [39] and GRSV95 [68] for $q(x)$ and $\Delta q(x)$, respectively, are used.

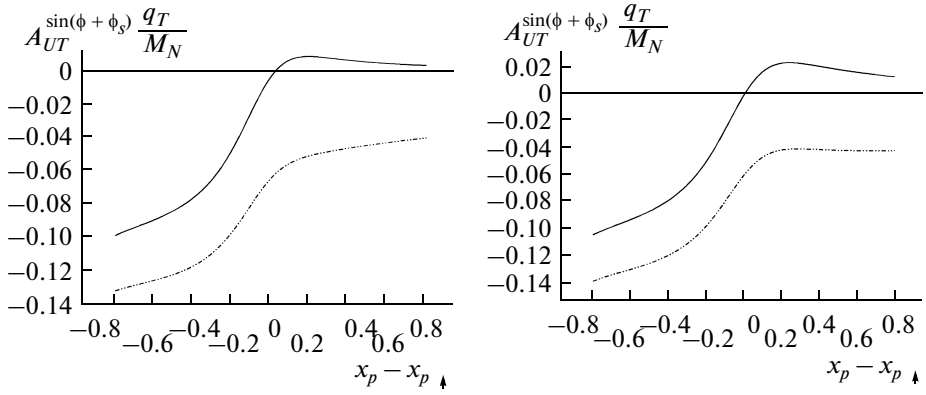

Fig. 4.4. Estimate of asymmetry $A_{UT}^{\sin(\phi+\phi_S)\frac{q_T}{M}}\Big|_{pp^\uparrow}$ for NICA, $s = 400^2$ GeV^2 for $Q^2 =$ (left panel) 4 and (right panel) 15 GeV^2. Solid and dashed lines correspond to two versions of evolution model (4.26) and (4.27) for transversity. Parameterizations GRV94 [39] and GRSV95 [68] for $q(x)$ and $\Delta q(x)$, respectively, are used.

values of $A_{UT}^{\sin(\phi-\phi_S)\frac{q_T}{M}}$ with a fixed target it is necessary either to overcome constraint (4.24) using the "forward–backward" spectrometer for the unpolarized beam/polarized target option, or, in the case of the "forward" spectrometer geometry (constraint (4.24) holds) consider the polarized beam/unpolarized target option. Unfortunately both these variants are hardly possible for COMPASS where the "forward" spectrometer is used and the proton beam's polarization is not planned. At the same time, the option with the polarized proton beam is at present planned at the accelerator complex J-PARC [34].

To conclude this section, let us evaluate the approximations determined by formulas (4.10)–(4.13) in the case $x_p \gg x_{p^\uparrow}$, and (4.15)–(4.18) in the case $x_p \ll x_{p^\uparrow}$. These evaluations are very important for analysis, since these approximations allow one to reduce the set of additional unknown variables included in the equations for the measured asymme-

Table 4.1. NICA kinematics. The values of the asymmetry $A_{UT}^{\sin(\phi-\phi_S)\frac{q_T}{M}}$ calculated using (4.7) (column "*A*") in comparison with two approximations determined by (4.10), (4.15) (column "*B*") and (4.12), (4.17) (column "*C*"), respectively. Parameterization from [3] is used for f_{1T}

$s = 400$ GeV^2, $Q^2 = 4$ GeV^2				$s = 400$ GeV^2, $Q^2 = 15$ GeV^2			
$x_p - x_{p^\uparrow}$	*A*	*B*	*C*	$x_p - x_{p^\uparrow}$	*A*	*B*	*C*
–0.4000	0.0189	0.0184	0.0277	–0.4000	0.0178	0.0170	0.0277
–0.5000	0.0131	0.0129	0.0190	–0.5000	0.0132	0.0129	0.0204
–0.6000	0.0087	0.0086	0.0125	–0.6000	0.0093	0.0093	0.0142
–0.7000	0.0053	0.0053	0.0076	–0.7000	0.0061	0.0061	0.0091
–0.8000	0.0028	0.0028	0.0040	–0.8000	0.0033	0.0033	0.0049
0.4000	0.0514	0.0525	0.0614	0.4000	0.0828	0.0849	0.0984
0.5000	0.0486	0.0491	0.0556	0.5000	0.0811	0.0820	0.0922
0.6000	0.0460	0.0462	0.0509	0.6000	0.0788	0.0792	0.0867
0.7000	0.0437	0.0438	0.0471	0.7000	0.0764	0.0765	0.0818
0.8000	0.0417	0.0418	0.0439	0.8000	0.0742	0.0742	0.0775

tries. The corresponding calculations of the asymmetry $A_{UT}^{\sin(\phi-\phi_S)\frac{q_T}{M}}$ are given[18] in Table 4.1. It can be seen from this table that approximations (4.10) and (4.15) obtained by elimination of sea contributions for large x work very well (column "B"). At the same time, the agreement of the results obtained using double approximations (4.12) and (4.17) (column "C") with results in column "A" is not so good (but still quite acceptable). This is not surprising, since for applied parameterizations (3.42)–(3.44) for the Sivers functions [2, 3] the following equality holds:

$$f_{1T}^{\perp(1)u} = -f_{1T}^{\perp(1)d}, \tag{4.28}$$

this equality is substantiated in the framework of the $1/N_c$ expansion [46, 47].

On the other hand, in the case of asymmetry $A_{UT}^{\sin(\phi-\phi_S)\frac{q_T}{M}}$ both approximations (4.11), (4.13), and (4.16), (4.18) are quite good (see Table 4.2).

Thus, for the kinematic region $x_p \gg x_{p^\uparrow}$, approximation (4.10) can be safely used for obtaining the first moments of the Sivers functions for sea quarks. Concerning approximation (4.12), one should be more cautious: if indeed $f_{1T}^{\perp(1)u} \simeq -f_{1T}^{\perp(1)d}$, double approximation (4.12) is applicable, rather, for preliminary rough estimates. At the same time, the transversity and the Boer–Mulders functions for $x_p \gg x_{p^\uparrow}$ cannot be extracted, since the asymmetry $A_{UT}^{\sin(\phi-\phi_S)\frac{q_T}{M}}$ is negligible in this kinematic region. We recall that for the fixed target mode this region corresponds to the option with the unpolarized beam and the polarized target (if the "forward" spectrometer is considered, see (4.24)).

Let us consider the other limit $x_p \ll x_{p^\uparrow}$ which in the fixed target case and the forward geometry spectrometer corresponds to the option with the polarized beam and the unpolarized target. In this case we have the opposite situation: the asymmetry $A_{UT}^{\sin(\phi-\phi_S)\frac{q_T}{M}}$ assumes rather large values (and is presumably measurable). It was just shown that in this limit even the double approximation (4.18) can be used. This provides an interesting possibility of extracting the ratio $h_{1u}/h_{1u}^{\perp(1)}$ directly without a fitting procedure that includes a set of assumptions for the additional unknown variables.

4.2. Asymmetry in pD and DD Collisions

As usual, the application of the deuteron beam (deuteron target) along with the proton beam (proton target) allows one to simultaneously find the parton's distribution functions for *u* and *d* flavors in the proton.

Applying the $SU_f(2)$ symmetry to the results of the previous section, the corresponding results for the asymmetries in the case of Drell–Yan processes in *pD* and *DD* collisions can be easily obtained. Thus, for the asymmetries providing access to the first moments of

[18] For brevity we present just two tables for NICA kinematics. Our calculations show that for all other considered kinematic conditions (RHIC, COMPASS, and J-PARC) the obtained results are absolutely similar.

Table 4.2. NICA kinematics. The values of the asymmetry $A_{UT}^{\sin(\phi+\phi_S)\frac{q_T}{M}}$ calculated using (4.6) (column "A") in comparison with two approximations determined by (4.11), (4.16) (column "B") and (4.13), (4.18) (column "C"), respectively. The evolution model with the following initial conditions is used for the transversity: $h_{1q(\bar{q})} = \Delta q(\bar{q})$ for $Q_0^2 = 0.23$ GeV^2

$s = 400$ GeV^2, $Q^2 = 4$ GeV^2				$s = 400$ GeV^2, $Q^2 = 15$ GeV^2			
$x_p - x_{p^\uparrow}$	A	B	C	$x_p - x_{p^\uparrow}$	A	B	C
−0.4000	−0.0761	−0.0800	−0.0912	−0.4000	−0.0783	−0.0833	−0.0951
−0.5000	−0.0838	−0.0856	−0.0948	−0.5000	−0.0864	−0.0887	−0.0983
−0.6000	−0.0894	−0.0902	−0.0975	−0.6000	−0.0926	−0.0936	−0.1012
−0.7000	−0.0940	−0.0943	−0.1000	−0.7000	−0.0980	−0.0984	−0.1041
−0.8000	−0.0987	−0.0988	−0.1029	−0.8000	−0.1038	−0.1039	−0.1078
0.4000	0.0063	0.0067	0.0068	0.4000	0.0200	0.0216	0.0220
0.5000	0.0052	0.0054	0.0054	0.5000	0.0176	0.0184	0.0186
0.6000	0.0044	0.0045	0.0045	0.6000	0.0156	0.0159	0.0160
0.7000	0.0038	0.0038	0.0038	0.7000	0.0138	0.0139	0.0140
0.8000	0.0033	0.0033	0.0033	0.8000	0.0123	0.0124	0.0124

the Sivers function in limiting case (4.9) we immediately obtain instead of (4.10) the following formulas:

$$A_{UT}^{\sin(\phi-\phi_S)\frac{q_T}{M}}(x_D \gg x_{p^\uparrow})\Big|_{Dp^\uparrow \to l^+l^-X} \simeq 2\frac{4\bar{f}_{1T}^{\perp(1)u}(x_{p^\uparrow}) + \bar{f}_{1T}^{\perp(1)d}(x_{p^\uparrow})}{4\bar{f}_{1u}(x_{p^\uparrow}) + \bar{f}_{1d}(x_{p^\uparrow})}, \tag{4.29}$$

and

$$A_{UT}^{\sin(\phi-\phi_S)\frac{q_T}{M}}(x_p \gg x_{D^\uparrow})\Big|_{pD^\uparrow \to l^+l^-X} = A_{UT}^{\sin(\phi-\phi_S)\frac{q_T}{M}}(x_D \gg x_{D^\uparrow})\Big|_{DD^\uparrow \to l^+l^-X} \simeq 2\frac{\bar{f}_{1T}^{\perp(1)u}(x_{D^\uparrow}) + \bar{f}_{1T}^{\perp(1)d}(x_{D^\uparrow})}{\bar{f}_{1u}(x_{D^\uparrow}) + \bar{f}_{1d}(x_{D^\uparrow})}, \tag{4.30}$$

whereas, in limiting case (4.14) we have

$$A_{UT}^{\sin(\phi-\phi_S)\frac{q_T}{M}}(x_D \gg x_{p^\uparrow})\Big|_{Dp^\uparrow \to l^+l^-X} \simeq 2\frac{4f_{1T}^{\perp(1)u}(x_{p^\uparrow}) + f_{1T}^{\perp(1)d}(x_{p^\uparrow})}{4f_{1u}(x_{p^\uparrow}) + f_{1d}(x_{p^\uparrow})}, \tag{4.31}$$

and

$$A_{UT}^{\sin(\phi-\phi_S)\frac{q_T}{M}}(x_p \gg x_{D^\uparrow})\Big|_{pD^\uparrow \to l^+l^-X} = A_{UT}^{\sin(\phi-\phi_S)\frac{q_T}{M}}(x_D \gg x_{D^\uparrow})\Big|_{DD^\uparrow \to l^+l^-X} \simeq 2\frac{f_{1T}^{\perp(1)u}(x_{D^\uparrow}) + f_{1T}^{\perp(1)d}(x_{D^\uparrow})}{f_{1u}(x_{D^\uparrow}) + f_{1d}(x_{D^\uparrow})}. \tag{4.32}$$

At the same time, the asymmetry providing information on the transversity and the first moment of the Boer–Mulders function assumes the form

$$A_{UT}^{\sin(\phi-\phi_S)\frac{q_T}{M}}(x_D \ll x_{p^\uparrow})\Big|_{Dp^\uparrow \to l^+l^-X} \simeq -\frac{[h_{1u}^{\perp(1)}(x_D) + h_{1d}^{\perp(1)}(x_D)][4\bar{h}_{1u}(x_{p^\uparrow}) + \bar{h}_{1d}(x_{p^\uparrow})]}{[f_{1u}(x_D) + f_{1d}(x_D)][4\bar{f}_{1u}(x_{p^\uparrow}) + \bar{f}_{1d}(x_{p^\uparrow})]}, \tag{4.33}$$

$$A_{UT}^{\sin(\phi-\phi_S)\frac{q_T}{M}}(x_D \gg x_{p^\uparrow})\Big|_{Dp^\uparrow \to l^+l^-X} \simeq -\frac{[4h_{1u}^{\perp(1)}(x_p) + h_{1d}^{\perp(1)}(x_p)][\bar{h}_{1u}(x_{D^\uparrow}) + \bar{h}_{1d}(x_{D^\uparrow})]}{[4f_{1u}(x_p) + f_{1d}(x_p)][\bar{f}_{1u}(x_{D^\uparrow}) + \bar{f}_{1d}(x_{D^\uparrow})]}, \tag{4.34}$$

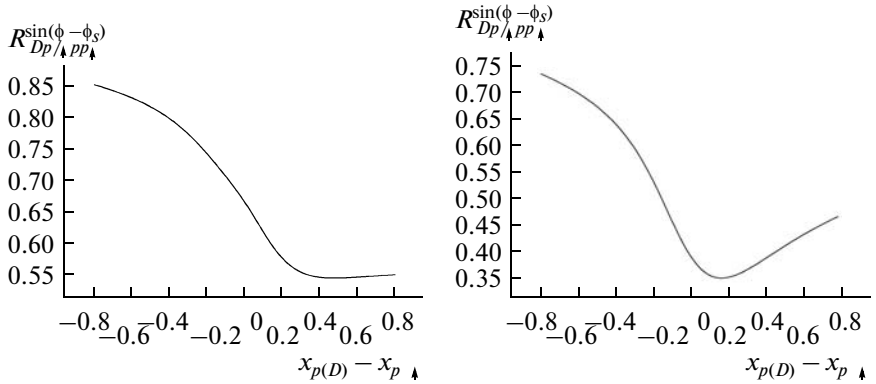

Fig. 4.5. Estimate of ratio $R = A_{UT}^{\sin(\phi-\phi_S)\frac{q_T}{M}}\Big|_{Dp^\uparrow} / A_{UT}^{\sin(\phi-\phi_S)\frac{q_T}{M}}\Big|_{pp^\uparrow}$ for NICA kinematics with $Q^2 =$ (left panel) 4 and (right panel) 15 GeV^2.

and

$$A_{UT}^{\sin(\phi-\phi_S)\frac{q_T}{M}}(x_D \gg x_{D^\uparrow})\Big|_{DD^\uparrow\to l^+l^-X} \simeq -\frac{[h_{1u}^{\perp(1)}(x_D)+h_{1d}^{\perp(1)}(x_D)][\bar{h}_{1u}(x_{D^\uparrow})+\bar{h}_{1d}(x_{D^\uparrow})]}{[f_{1u}(x_D)+f_{1d}(x_D)][\bar{f}_{1u}(x_{D^\uparrow})+\bar{f}_{1d}(x_{D^\uparrow})]} \quad (4.35)$$

in limiting case (4.9), whereas

$$A_{UT}^{\sin(\phi-\phi_S)\frac{q_T}{M}}(x_D \ll x_{p^\uparrow})\Big|_{Dp^\uparrow\to l^+l^-X} \simeq -\frac{[4\bar{h}_{1u}^{\perp(1)}(x_D)+\bar{h}_{1d}^{\perp(1)}(x_D)][h_{1u}(x_{p^\uparrow})+h_{1d}(x_{p^\uparrow})]}{[\bar{f}_{1u}(x_D)+\bar{f}_{1d}(x_D)][f_{1u}(x_{p^\uparrow})+f_{1d}(x_{p^\uparrow})]}, \quad (4.36)$$

$$A_{UT}^{\sin(\phi-\phi_S)\frac{q_T}{M}}(x_D \ll x_{p^\uparrow})\Big|_{Dp^\uparrow\to l^+l^-X} \simeq -\frac{[4\bar{h}_{1u}^{\perp(1)}(x_p)+\bar{h}_{1d}^{\perp(1)}(x_p)][h_{1u}(x_{D^\uparrow})+h_{1d}(x_{D^\uparrow})]}{[\bar{f}_{1u}(x_p)+\bar{f}_{1d}(x_p)][f_{1u}(x_{D^\uparrow})+f_{1d}(x_{D^\uparrow})]}, \quad (4.37)$$

and

$$A_{UT}^{\sin(\phi-\phi_S)\frac{q_T}{M}}(x_D \ll x_{p^\uparrow})\Big|_{DD^\uparrow\to l^+l^-X} \simeq -\frac{[\bar{h}_{1u}^{\perp(1)}(x_D)+\bar{h}_{1d}^{\perp(1)}(x_D)][h_{1u}(x_{D^\uparrow})+h_{1d}(x_{D^\uparrow})]}{[\bar{f}_{1u}(x_D)+\bar{f}_{1d}(x_D)][f_{1u}(x_{D^\uparrow})+f_{1d}(x_{D^\uparrow})]} \quad (4.38)$$

in limiting case (4.14).

It was already noted (see the previous section) that there exist strong theoretical arguments [46, 47] in favor of satisfaction of equality (4.28), i.e., it can be expected that the measured sum $f_{1T}^{\perp(1)u} + f_{1T}^{\perp(1)d}$ of the first moments of the Sivers functions of u and d flavors will be very small.[19] Moreover, QCD evolution predicts small sea distributions for transversity even for small values of x [28]. Thus, in the case of the polarized deuteron in the initial state almost all corresponding asymmetries (see (4.30), (4.32), (4.34), and (4.35)) presumably should be very small (our calculations prove it), comparable with zero within errors (of course, it should be thoroughly verified by corresponding measurements at RHIC, NICA, COMPASS, and J_PARC). Only asymmetries with a polarized deuteron which in principle could take nonzero values containing the sum $h_{1u}(x_{D^\uparrow}) + h_{1d}(x_{D^\uparrow})$ (see (4.37) and (4.38)). The matter is that the analysis of COMPASS data [43] on semi-inclusive deep inelastic scattering on the deuteron target performed in [4] showed that it is possible that this sum is nonzero. According to the results of [4], the central values of the parton's distribution functions h_{1u} and h_{1d} have opposite signs and their absolute values are not equal.[20] However, the uncertainties for h_{1u} and h_{1d} are too large (see the error band in Fig. 7) to make the unambiguous conclusion whether $h_{1u} + h_{1d}$ is equal to zero or not. Thus, only new measurements can give the final answer to this question; among these measurements the most promising ones are the planned measurements of single-spin asymmetries in Drell–Yan processes with a polarized deuteron.

Our calculations show that, unlike the case of polarized deuterons, for polarized protons in the initial state, all asymmetries can assume rather large values comparable with the values of the corresponding asymmetries in the case of $pp^\uparrow$ collisions, (see Figs. 4.5, 4.6.)

[19] Taking into account assumption (4.23) this means that the sum $\bar{f}_{1T}^{\perp(1)u} + \bar{f}_{1T}^{\perp(1)d}$ of the first moments of the Sivers parton's distribution function of sea u and d quarks should also be very small.

[20] The evolution model consistent with the results of [4] (see discussion of Fig. 4.2) also predicts that $h_{1u} \neq h_{1d}$.

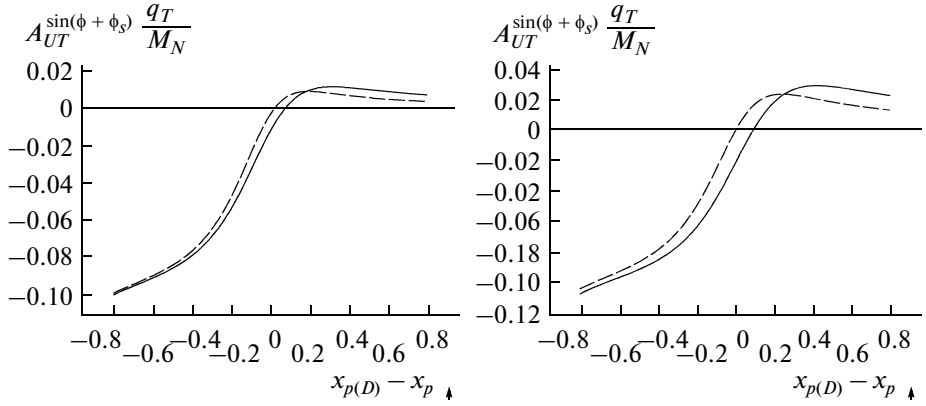

Fig. 4.6. Estimate of asymmetry $A_{UT}^{\sin(\phi+\phi_S)\frac{q_T}{M}}$ for NICA for (dashed line) $pp^{\uparrow}$ and (solid line) $Dp^{\uparrow}$ collisions and $Q^2 =$ (left panel) 4 and (right panel) 15 GeV^2. Evolution model with initial conditions (4.27) is used for h_{1q}. Parameterizations GRV94 [39] and GRSV95 [68] for $q(x)$ and $\Delta q(x)$, respectively, are used.

For brevity we present the relations between the asymmetries for $pp^{\uparrow}$ and $Dp^{\uparrow}$ collisions only for NICA kinematics, since they practically do not differ from the corresponding relations for RHIC, COMPASS, and J-PARC kinematic conditions.

Figure 4.5 shows the ratio

$$R = A_{UT}^{\sin(\phi-\phi_S)\frac{q_T}{M}}\Big|_{Dp^{\uparrow}} / A_{UT}^{\sin(\phi-\phi_S)\frac{q_T}{M}}\Big|_{pp^{\uparrow}}.$$

This ratio (which is similar for all three employed parameterizations (3.42)–(3.44) varies from 0.4 to 0.8.

In Fig. 4.6 the asymmetry $A_{UT}^{\sin(\phi-\phi_S)\frac{q_T}{M}}$ is represented for $Dp^{\uparrow}$ and $pp^{\uparrow}$ collisions, and it can be seen that the corresponding curves practically coincide.

Thus, the conclusion can be made that in the case of $Dp^{\uparrow}$ collisions both asymmetries integrated with the angular weights $\sin(\phi - \phi_S)$ and $\sin(\phi + \phi_S)$ are presumably measurable in the same x regions as the corresponding asymmetries for $pp^{\uparrow}$ collisions.

5. ESTIMATES OF MEASURABILITY OF ASYMMETRIES WITH A NEW GENERATOR OF POLARIZED DRELL–YAN EVENTS

The generator of polarized Drell–Yan events is necessary, first, for estimation of asymmetry measurability at the preliminary (theoretical) stage (without account of specific features of the experimental setup) (see this section); second, as the basis for program packages for detector simulation (for example, such as GEANT-based codes [48]) at the stages of experimental setup design and analysis of experimental data. Until recently no Drell–Yan event generator, except for the PYTHIA generator [27], was available. Unfortunately, PYTHIA considers only unpolarized Drell–Yan events; moreover, this generation does not contain correct (in agreement with experimental data [17, 18]) q_T and $\cos 2\phi$ dependences of Drell–Yan cross sections, which is absolutely necessary for investigation of the Boer–Mulders effect.

The first generator of polarized Drell–Yan events [49, 50] with due account of q_T and angular dependences has appeared recently. In order to correct the defects of this generator, simplify introduction of new capabilities into the program, and effectively control all calculations, we developed [14] the alternative generator of polarized Drell–Yan events. The event generation scheme used in it is rather simple and is to a large extent similar to that used in the GMC_TRANS generator [51] that was successfully used by the collaboration HERMES for simulation of the Sivers effect in semi-inclusive deep inelastic scattering [5]. Briefly, this generation scheme for polarized Drell–Yan events can be described as follows. First, the generator chooses the flavor q of the annihilating $q\bar{q}$ pair and chooses, whether this hadron (for example, polarized one) contains the annihilating quark or, alternatively, the annihilating antiquark of the given (chosen) flavor. This is performed in accordance with the total unpolarized Drell–Yan cross sections for each flavor and each alternative (quark or antiquark annihilation) for the given hadron in the initial state. Then, the variables x_F and Q^2 are randomly sampled according to the part of cross section (2.12) of unpolarized process (2.1) which does not contain angular dependences. At the next step, the polar angle θ is randomly sampled according to the $\sin\theta(1 + \cos^2\theta)$ distribution in this cross section. Then, the Gaussian model for $f_{1q}(x, k_T)$ is applied, and the transverse momentum of the lepton pair q_T is randomly sampled according to the exponential distribution $\exp(-q_T^2/2)/2\pi$. At the next stage,

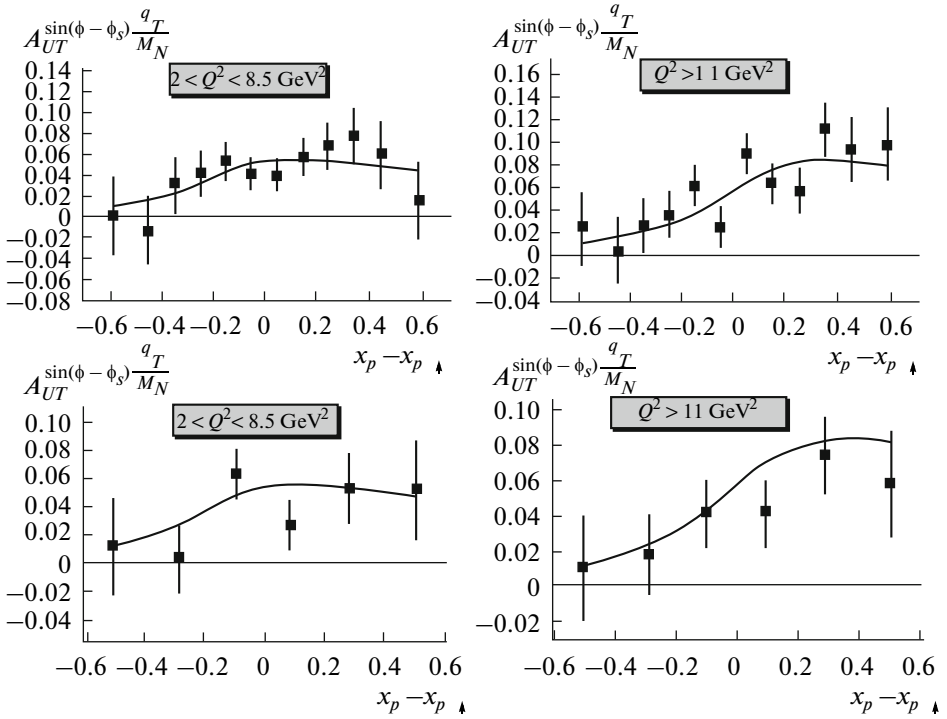

Fig. 5.1. Results of simulation of asymmetry $A_{UT}^{\sin(\phi-\phi_S)\frac{q_T}{M}}\Big|_{pp^\uparrow}$ for NICA, $s = 400$ GeV^2. Fit from [3] is used for the Sivers function. Points with error bars are obtained by simulation with polarized Drell–Yan event generator for statistics of (upper) 100000 and (lower) 50000 pure events; $\langle Q^2 \rangle$ (left panels) $\simeq 3.5$ and (right panels) $= 15$ GeV^2.

the angular variables ϕ and ϕ_S are sampled according to $\cos 2\phi$, $\sin(\phi - \phi_S)$, and $\sin(\phi + \phi_S)$ dependences of the cross section (2.13) of singly polarized process (2.2). In this case, the k_T-dependences of the Boer–Mulders $h_{1q}^{\perp}(x, k_T)$ and Sivers $f_{1T}^{q}(x, k_T)$ distributions are fixed using Boer model (2.15) and the Gaussian ansatz [2, 3], respectively. It is important that at this stage of simulation of the variables ϕ and ϕ_S, the variables x_F, Q^2, θ, and q_T have already been simulated,[21] which considerably increases the simulation rate for the angles ϕ and ϕ_S. All variables are generated using the standard von Neumann's "acceptance–rejection" method, see, e.g., [27].

We underline once more that the generator developed in [16, 49] is the first generator of polarized Drell–Yan events, and in many respects it helped us to write the new generator whose advantage will be described below.

It was already noted that one of the main requirements to any generator of polarized Drell–Yan events is the correct account of the nontrivial q_T-dependence of Drell–Yan cross sections. This is especially important for q_T-weighted objects considered here. In the generator [49, 50], the approximations for calculation of convolutions in $h_{1q}^{\perp}$-containing parts of cross sections (2.12) and (2.13) should be used similar to that done in [15] (see the discussion of formulas (47) and (53) in [15]). However, direct calculations show that the application of these approximations in the generator results in the considerable distortion of the values of q_T-weighted objects, such as the asymmetry $A_{UT}^{\sin(\phi-\phi_S)\frac{q_T}{M}}$: the values of asymmetry obtained from the simulated data essentially differ from the corresponding values calculated directly from the parameterizations/models for f_{1q}, $h_{1q}^{\perp}$, and h_{1q} embedded in the generator. That is why we avoid approximations of this type. Instead, we numerically calculate convolutions for a large discrete set of values of q_T and then perform the standard spline interpolation in order to recover the calculated convolution as the continuous function of q_T. As a result (see, e.g., Fig. 5.2), the values of $A_{UT}^{\sin(\phi-\phi_S)\frac{q_T}{M}}$ reconstructed from the simulated data are in good agreement with corresponding values calculated directly from the parameterizations/models for the distribution functions used in the generator.

[21] Of course, all variables can be simulated simultaneously, as it is done, for example, in [16, 49]. However, this scheme considerably reduces the event generation rate.

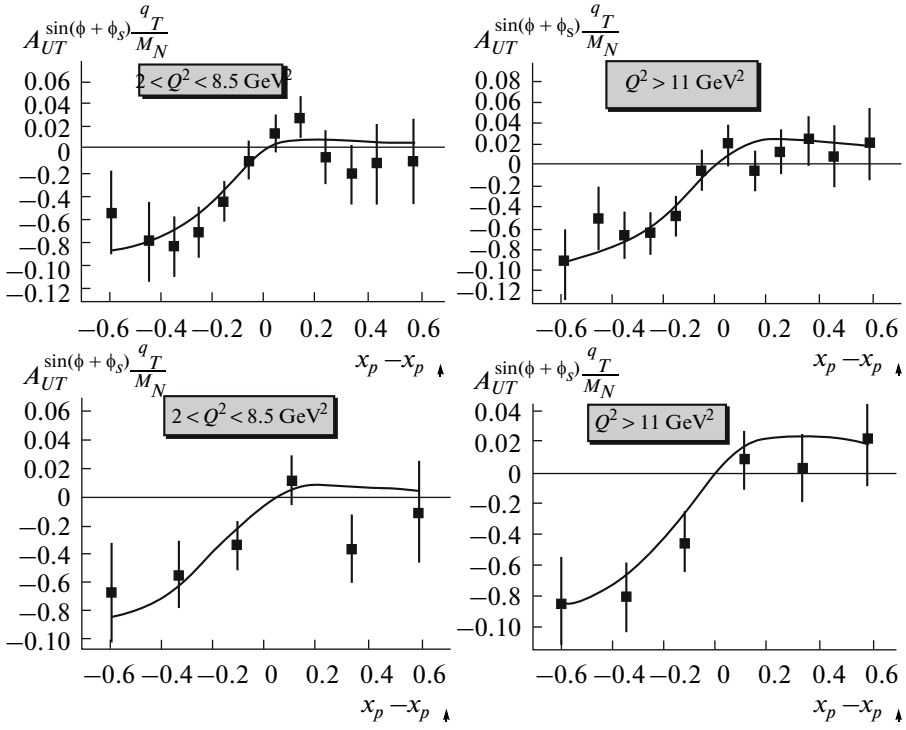

Fig. 5.2. Results of simulation of asymmetry $A_{UT}^{\sin(\phi+\phi_S)\frac{q_T}{M}}\Big|_{pp^\uparrow}$ for NICA, $s = 400$ GeV^2. Evolution model with initial conditions (4.27) is used for h_{1q}. Parameterizations GRV94 [39] and GRSV95 [68] for $q(x)$ and $\Delta q(x)$, respectively, are used. Points with error bars are obtained by simulation with polarized Drell–Yan event generator for statistics of (upper) 100000 and (lower) 50000 pure events; $\langle Q^2\rangle$ (left panels) $\simeq 3.5$ and (right panels) $= 15$ GeV^2.

Another important advantage of the new generator is that it can be much easier combined with the PYTHIA generator (which includes practically all possible processes), which is necessary for analysis of background processes that may yield false signals for Drell–Yan events. Unlike the generator [49, 50], in the new generator, similar to PYTHIA, Drell–Yan events are generated for each flavor separately. Note important technical advantages of the new generator: due to the good event generation scheme, the generation rate turns out to be much higher than for the generator [49, 50], in which all kinematic variables, are simulated simultaneously; the cross-section maxima for the von Neumann's algorithm are found automatically, similar to the calculation of the total cross sections at the end of each generation cycle.

Now that the efficient generator of polarized Drell–Yan events is available, the measurability of asymmetries calculated earlier can be estimated. Of course, these estimates should be considered as preliminary estimates of the first, theoretical level. In order to exhaustively estimate the measurability, it is necessary to take into account all specific features of a particular experimental setup.

Let us first present the estimates for Drell–Yan processes with protons and deuterons in the initial state. Two sets of simulated data corresponding to statistics of 100000 and 50000 pure Drell–Yan events were prepared, for each of the two regions of Q^2: $2 < Q^2 < 8.5$ GeV^2 and $Q^2 > 11$ GeV^2. The cut $2 < Q^2 < 8.5$ GeV^2 was applied in order to eliminate false identification of the lepton pair due to multiple background processes (combinatorial background from Dalitz decays and γ conversion, etc., see, e.g., Section F.4.2 in [52]) below $Q^2 = 2$ GeV^2, and also to eliminate lepton pairs from the region of J/ψ resonance. The cut $Q^2 > 11$ GeV^2 was also applied in order to avoid the region of J/ψ resonance. Similar to the above, we do not give estimates of measurability of the asymmetry $A_{UT}^{\sin(\phi-\phi_S)\frac{q_T}{M}}\Big|_{pp^\uparrow}$ for RHIC kinematics (they were already given in [3]). Thus, for this asymmetry we again (see Section 4.1) present the results for $\sqrt{s} = 20$ GeV typical for NICA keeping in mind that the results of calculation of $A_{UT}^{\sin(\phi-\phi_S)\frac{q_T}{M}}\Big|_{pp^\uparrow}$ for COMPASS and J-PARC (in comparison with RHIC, very close to NICA with respect to $\sqrt{s}$) are quite close (see Section 4.1) to the corresponding results for NICA. The results are shown in Fig. 5.1. For simulations with

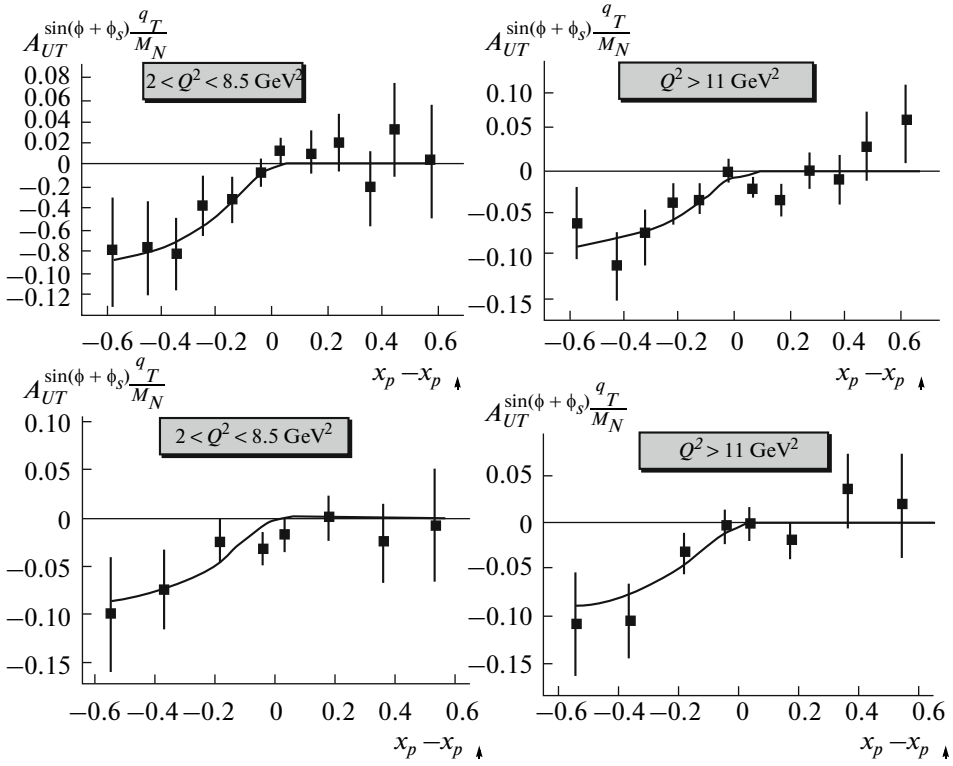

Fig. 5.3. Results of simulation of asymmetry $A_{UT}^{\sin(\phi+\phi_S)\frac{q_T}{M}}\Big|_{pp^\uparrow}$ for RHIC, $s = 200$ GeV^2. Evolution model with initial conditions (4.27) is used for h_{1q}. Parameterizations GRV94 [39] and GRSV95 [68] for $q(x)$ and $\Delta q(x)$, respectively, are used. Points with error bars are obtained by simulation with polarized Drell–Yan event generator for statistics of (upper) 100000 and (lower) 50000 pure events; $\langle Q^2\rangle$ (left panels) $\simeq 3.9$ and (right panels) $= 22$ GeV^2.

the new generator we used the last parameterization, fit III (solid line in Fig. 5.1) of the set of parameterizations (3.42)–(3.44).

It can be seen from Fig. 5.1 that even for relatively low statistics of 50000 of pure Drell–Yan events (lower part of Fig. 5.1) there are three presumably measurable points for $A_{UT}^{\sin(\phi-\phi_S)\frac{q_T}{M}}$ in the kinematic region $x_p - x_{p^\uparrow} > 0$ where this asymmetry assumes values of 4–6%. It can be seen that for statistics of 100000 events one can hope that the functional form of the asymmetry will be reconstructed (see upper part of Fig. 5.1) in the kinematic region $x_p > x_{p^\uparrow}$. Since the kinematic region $x_p > x_{p^\uparrow}$ corresponds to $x_F > 0$ for the option with the polarized target and unpolarized beam available for COMPASS and J-PARC, the conclusion can be made that all four experimental facilities RHIC, NICA, COMPAS, and J-PARC can provide access to the Sivers function (see Section 4.1). At the same time, in the region $x_p < x_{p^\uparrow}$ available for RHIC, NICA, and (presumably) J-PARC, the asymmetry $A_{UT}^{\sin(\phi-\phi_S)\frac{q_T}{M}}$ turns out to be lower (smaller than 4%), but can still be observed within errors (even for statistics of 50000 events, at least one measurable point can be seen).

Let us consider the measurability of the Sivers effect in the case of the deuteron in the initial state. It can be concluded from Figs. 4.5 and 5.1 that the only asymmetry of this kind $A_{UT}^{\sin(\phi-\phi_S)\frac{q_T}{M}}\Big|_{Dp^\uparrow}$ that can assume sufficiently large values (see Section 4.1) is hardly measurable for statistics of 50000 pure Drell–Yan events. At the same time, for statistics of 100000 events this asymmetry becomes presumably measurable.

Let us estimate the measurability of the asymmetry $A_{UT}^{\sin(\phi-\phi_S)\frac{q_T}{M}}$ which gives access to the transversity and the Boer–Mulders distribution. We again present (see Section 4.1) the estimates for $pp^\uparrow$ collisions and two considerably different values of $\sqrt{s}$ corresponding to RHIC and NICA kinematic conditions. These results are shown in Figs. 5.2 and 5.3. For $\sqrt{s}$ corresponding to COMPASS and J-PARC kinematic conditions our calculations yield almost the same results as for NICA kinematics; therefore, it is not necessary to give them

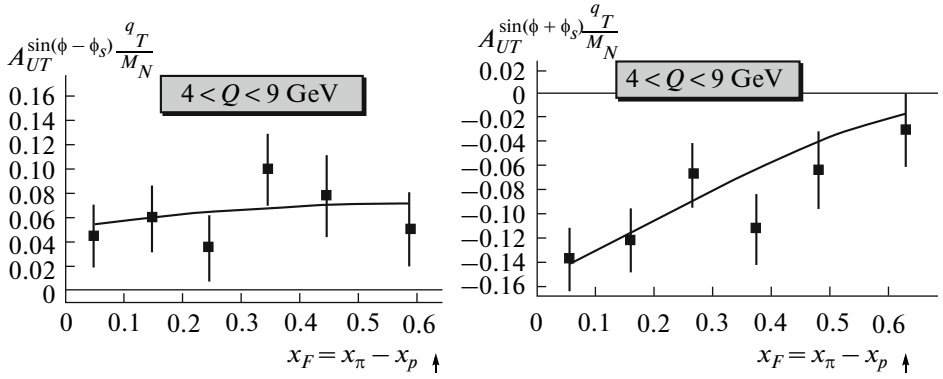

Fig. 5.4. Estimates of measurability of asymmetries (left panel) $A_{UT}^{\sin(\phi-\phi_S)\frac{q_T}{M}}\Big|_{pp^\uparrow}$ and (right panel) $A_{UT}^{\sin(\phi+\phi_S)\frac{q_T}{M}}\Big|_{pp^\uparrow}$ for COMPASS, $s =$ 300 GeV^2. Fit from [3] for the Sivers function is used for (solid lines) theoretical estimates of asymmetries, evolution model with initial conditions (4.27) for h_{1q}, Boer model (2.15) for $h_{1q}^{\perp(1)}$, parameterization [64] for $f_{1q}\big|_{\pi^-}$, parameterization GRV94 [39] for $f_{1q}\big|_p$, parameterization GRSV95 [68] for $\Delta q|_p$ are used. Points with error bars are obtained by simulation with polarized Drell–Yan event generator for statistics of 50000 pure events and $\langle Q^2\rangle \simeq 25$ GeV^2 for both figures.

here. For simulations with the new generator we again use (see Section 4.1) the Boer model (2.15) for $h_1^\perp$ and the evolution model with initial conditions (4.27).

It can be seen from Figs. 5.2 and 5.3 that in the region $x_p < x_{p^\uparrow}$, even for relatively low statistics of 50000 pure Drell–Yan events (lower part of Fig. 5.2), one can hope that at least three points for the asymmetry $A_{UT}^{\sin(\phi-\phi_S)\frac{q_T}{M}}$ can be observed within errors. At the same time, for statistics of 100000 events, probably, the functional form of this asymmetry can be reconstructed (see upper part of Fig. 5.2) in the region $x_p < x_{p^\uparrow}$. Unfortunately, the kinematic region $x_p < x_{p^\uparrow}$ is hardly achievable for COMPASS due to the "forward" spectrometer's geometry and the unpolarized proton beam of this running experiment. In the case of another fixed target experiment planned at the J-PARC accelerator complex this region could be achieved in the case of the polarized proton beam (at present, this option is planned at J-PARC [34]). It is very important that in the symmetric collider mode (RHIC and NICA) there are no problems with achieving the region $x_p < x_{p^\uparrow}$.

Note that since the values of $A_{UT}^{\sin(\phi+\phi_S)\frac{q_T}{M}}$ in the cases of $pp^\uparrow$ and $Dp^\uparrow$ collisions are close (see Fig. 4.6) all conclusions concerning the measurability of this asymmetry in the first case can be automatically applied to the second case.

Finalizing the discussion of Figs. 5.1–5.3, it is reasonable to make the following important remark. It can be seen from these figures that even if the experimentally available statistics of Drell–Yan events turns out to be relatively low (smaller than 50000 events), probably, it would be hardly possible to reconstruct the functional forms of the first moments of the Sivers and Boer–Mulders distributions. However, even in the case of this unfavorable situation one can hope that it would be possible at least to verify the fundamental QCD predictions (1.1) and (1.2) for these distributions.

To conclude this section, let us estimate the measurability of the asymmetries $A_{UT}^{\sin(\phi-\phi_S)\frac{q_T}{M}}$ and $A_{UT}^{\sin(\phi+\phi_S)\frac{q_T}{M}}$ for Drell–Yan processes $\pi^- p^\uparrow \to \mu^+\mu^- X$ available for COMPASS. The optimal kinematic conditions for the COMPASS program concerning these processes were chosen not long ago [35]. They are the pion's beam energy of 160 GeV and the range $4 < Q < 9$ GeV for the invariant mass of the dilepton pair. The results of theoretical calculations of the asymmetries $A_{UT}^{\sin(\phi\pm\phi_S)\frac{q_T}{M}}\Big|_{\pi^- p^\uparrow}$ and their simulation with the new generator for these kinematical conditions are shown in Fig. 5.4. Due to constraint (4.24) for the "forward" spectrometer available at COMPASS we present the results of calculations in the region $x_\pi > x_{p^\uparrow}$. It can be seen from Fig. 5.4 that even for relatively low statistics of 50000 events there are six presumably measurable points for each of the asymmetries, which allows one to hope that it would be possible to reconstruct the functional forms of both asymmetries even for not very favorable data taking conditions. Thus, the conclusion can be made that for COMPASS it is much more preferable to study Drell–Yan processes in pion–proton colli-

sions. At the same time, as it was discussed above, the processes $p(D)p^{\uparrow}(D^{\uparrow}) \to l^+l^-X$ can be most efficiently studied in the collider mode at RHIC and NICA.

6. DUALITY OF DRELL–YAN AND J/ψ PRODUCTION PROCESSES

At present, the increasing interest [53–55] to the close analogy (duality) of the mechanisms of Drell–Yan $H_1H_2 \to \gamma^*X \to l^+l^-X$ and J/ψ resonance production processes with the J/ψ dilepton's decay mode $H_1H_2 \to J/\psi X \to l^+l^-X$ (see monograph [56] for details) is observed. It is assumed that this analogy/duality takes place for relatively low energies when the J/ψ production mechanism, due to the quark–antiquark ($\bar{q}q$) fusion mechanism, considerably dominates over the quark–gluon (gg) fusion mechanism. Then, since J/ψ is the vector particle, similar to the γ quantum, the helicity structure of interactions $\bar{q}q\,(J/\psi)$ and $(\bar{q}q)\gamma^*$ is similar, and the J/ψ production's cross section can be obtained from the cross section of the Drell–Yan processes using the simple substitution,

$$16\pi^2\alpha^2 e_q^2 \to (g_q^{J/\psi})^2 (g_l^{J/\psi})^2,$$
$$\frac{1}{M^4} \to \frac{1}{(M^2 - M_{J/\psi}^2)^2 + M_{J/\psi}^2\Gamma_{J/\psi}^2}, \qquad (6.1)$$

where $M^2 \equiv Q^2$ is the squared invariant mass of the lepton pair, $M_{J/\psi}^2 \simeq 9.59$ GeV^2 is the squared J/ψ mass, and $\Gamma_{J/\psi}$ is the total width of J/ψ decay. It is assumed that model (6.1) is applicable both in unpolarized [54] and polarized [53] cases. The latter is substantiated by the identical character of the helicity and vector structure of elementary channels for the γ^* quantum and J/ψ (similitude of all γ^μ interactions). In particular, the model determined by (6.1) was used in [53] in the case of transverse polarization of both hadrons in the initial state.

Here, it should be noted that although it seems that the pure vector γ_μ interaction (Dirac interaction) is typical for J/ψ production this is still a hypothesis. In principle, other effects caused by $\sigma_{\mu\nu}$ interaction (Pauli interaction) are possible. It will be shown below that for a large number of processes with different unpolarized hadrons in the initial state, model (6.1), based on the pure vector interaction indeed works well at low energies. This can be considered as a strong argument in favor of the mechanism of pure vector interaction. At the same time, in the polarized case experimental data necessary for verification of the hypothesis of pure vector interaction are still absent. Thus, for comprehensive verification of the "duality" model (6.1) it is fundamentally important to obtain experimental data on Drell–Yan and J/ψ production processes in collisions of polarized hadrons. This is a strong additional motivation for such experiments which are at present planned at GSI, COMPASS, RHIC, NICA, and J-PARC experimental facilities.

The main advantage of model (6.1) is that in the region of u quark dominance (large values of the Bjorken variable x), all interaction constants in the cross-section ratios (such as asymmetries) are exactly cancelled, and as a result, they become absolutely identical for Drell–Yan and J/ψ production processes (see (23) in [53] and (10) in [54]). Thus, in this kinematic region it is not important which of the two processes is responsible for the production of the detected lepton pair near the J/ψ production's threshold for extraction of the parton's distribution functions. Of course, this possibility of using J/ψ production for extraction of the parton's distribution functions is very attractive, since the intensity of lepton pair's production in the region of J/ψ resonance is higher by two orders of magnitude than in the region above the J/ψ mass. In particular, the "duality" model (6.1) allows one to considerably decrease statistical errors for the transversity h_{1u} and the first moment of the Boer–Mulders distribution $h_{1u}^{\perp(1)}$ due to the fact that it is possible not to distinguish the data on Drell–Yan and J/ψ production processes obtained in the region of J/ψ resonance for analysis. Indeed, in the region of large x (u quark's dominance region), according to (6.1), the formulas determining $\hat{k}$ for both unpolarized processes (2.1) and

$$H_1H_2 \to J/\psi X \to l^+l^-X, \qquad (6.2)$$

and $\hat{A}_h$ for both singly polarized processes (2.2) and

$$H_1H_2^{\uparrow} \to J/\psi X \to l^+l^-X, \qquad (6.3)$$

look absolutely similar (compare with (2.21) and (2.28)),

$$\hat{k} = 8\frac{h_{1\bar{u}}^{\perp(1)}(x_1)\big|_{H_1} h_{1u}^{\perp(1)}(x_2)\big|_{H_2} + (u \leftrightarrow \bar{u})}{f_{1\bar{u}}(x_1)\big|_{H_1} f_{1u}(x_2)\big|_{H_2} + (u \leftrightarrow \bar{u})}, \qquad (6.4)$$

$$\hat{A}_h = -\frac{1}{2}\frac{h_{1\bar{u}}^{\perp(1)}(x_1)\big|_{H_1} h_{1u}^{\perp(1)}(x_2)\big|_{H_2^{\uparrow}} + (u \leftrightarrow \bar{u})}{f_{1\bar{u}}(x_1)\big|_{H_1} f_{1u}(x_2)\big|_{H_2^{\uparrow}} + (u \leftrightarrow \bar{u})}, \qquad (6.5)$$

which provides access to h_{1u} and $h_{1u}^{\perp(1)}$ as a result of the combined data analysis (analysis of angular and momentum distributions of the lepton pair) for both processes.

Of course, duality model (6.1) is applicable only for those kinematic regions, for which among elementary processes contributing to J/ψ production, quark–antiquark fusion dominates over gluon–gluon fusion. It is clear from qualitative considerations that gluon contributions are suppressed at low energies: for fixed Q^2 (9.6 GeV^2 for processes (6.2), (6.3)) x increases with decreasing $s \equiv (p_{H_1} + p_{H_2})^2$, while the ratio $g(x)/q(x)$ sharply decreases with increasing x. Nonetheless, quantitative analysis is necessary for determi-

nation of the region where gluon contributions can be safely neglected. This analysis was performed in [55]. For this purpose, along with model (6.1), the most popular well grounded J/ψ model is used; this model includes both elementary processes, quark–antiquark and gluon–gluon fusion; it is assumed to be good for any energies of colliding hadrons (see [57] and references therein). Then, the predictions of both models are compared with the corresponding experimental data from [58, 59].

In order to cancel the unknown J/ψ interaction constants we use the ratios,[22] rather than absolute values of cross sections of processes (6.2) with different hadrons/nuclei in the initial state. Namely, we consider the ratios of the J/ψ production's cross sections integrated over the angles and x_F (integration over x_F is performed in the front hemisphere, $x_F > 0$) of the form $\sigma_{pp}/\sigma_{\pi^\pm p}$, $\sigma_{pA}/\sigma_{\pi^\pm A}$, and $\sigma_{pp}/\sigma_{\bar{p}p}$, where the symbol A denotes different target nuclei (here, W, C, Ca, Cu, and Pt). The matter is that hadrons $\pi^\pm$ and $\bar{p}$, unlike the proton and other nuclei, contain the antiquark in the valence state. That is why it is very useful to study the ratios, such as $\sigma_{pp}/\sigma_{\pi^\pm p}$ and $\sigma_{pp}/\sigma_{\bar{p}p}$ which should demonstrate a very specific behavior: on the one hand, they should sharply decrease with decreasing s (large x, and valence quark/antiquark dominance region), and on the other hand, they should increase up to unity with increasing s (small x, dominance region of sea quarks and gluons). The largest amount of experimental data on J/ψ production, which provide access to such ratios, are those for the front hemisphere with respect to x_F for pion, antiproton, and proton beams colliding with proton or nuclear targets [58, 59].

Simple duality model (6.1), as applied to the ratios of cross sections $[\sigma_{H_1H_2}/\sigma_{H_1'H_2}]_{x_F>0}$, yields

$$[\sigma_{H_1H_2}/\sigma_{H_1'H_2}]_{x_F>0} = \frac{\int_0^{1-m^2_{J/\psi}/s} dx_F[s(x_1+x_2)]^{-1}F^{H_1H_2}_{q\bar{q}}}{\int_0^{1-m^2_{J/\psi}/s} dx_F[s(x_1+x_2)]^{-1}F^{H_1'H_2}_{q\bar{q}}}, \quad (6.6)$$

where the quark–antiquark flux $F^{H_1H_2}_{q\bar{q}}$ has the form

$$F^{H_1H_2}_{q\bar{q}} = \sum_{q=u,d,s}[q^{H_1}(x_1)\bar{q}^{H_2}(x_2) + \bar{q}^{H_1}(x_1)q^{H_2}(x_2)], \quad (6.7)$$

while the Bjorken variables $x_{1,2}$ are expressed in terms of the Feynman variable $x_F = x_1 - x_2$ as

$$x_{1,2} = [\pm x_F + \sqrt{x_F^2 + 4m^2_{J/\psi}/s}]/2.$$

[22] We recall that the main objective is the investigation of the ratios, asymmetries, which provide access to a different parton's distribution functions.

Note that the ratios $g_d^{J/\psi}/g_u^{J/\psi}$ and $g_s^{J/\psi}/g_u^{J/\psi}$ were assumed equal to unity in accordance with available experimental data [60] upon obtaining (6.6) and (6.7). Indeed, data [60] obtained for the absolutely symmetric (the cross section per one nucleon has the form $\sigma_{\pi^\pm C} = [\sigma_{\pi^\pm p} + \sigma_{\pi^\pm n}]/2$) carbon target clearly demonstrate that the ratio $\sigma_{\pi^+C}/\sigma_{\pi^-C}$ is close to unity in the region of J/ψ resonance, while for large lepton pair's mass it drops to 1/4 (see Fig. 2 in [60] and discussion of this figure). This is a very good argument in favor of the fact that, unlike the $q\bar{q}$ pair's annihilation mechanism for the Drell–Yan process (where the d quark is suppressed by the charge factor $e_d^2/e_u^2 = 1/4$), for J/ψ production u and d quarks should be symmetrically included in the cross sections with the same charge factor,

$$g_d^{J/\psi}/g_u^{J/\psi} \simeq 1.$$

We also use the similar relation

$$g_s^{J/\psi}/g_u^{J/\psi} \simeq 1,$$

taking into account that the quadratic contributions of the sea's strange quarks into the cross sections are rather small.

The fundamental difference of the "gluon evaporation" model from model (6.1) is that the former, along with the contribution from $q\bar{q}$ fusion $F^{H_1H_2}_{qq}$ determined by (6.7) contains the contribution

$$F^{H_1H_2}_{gg} = g^{H_1}(x_1)g^{H_2}(x_2),$$

corresponding to the gluon–gluon fusion. If the "gluon evaporation" model is applied to the ratios $[\sigma_{H_1H_2}/\sigma_{H_1'H_2}]_{x_F>0}$, it yields

$$\frac{\sigma_{H_1H_2}\big|_{x_F>0}}{\sigma_{H_1'H_2}\big|_{x_F>0}} = \frac{(\sigma_{q\bar{q}}+\sigma_{gg})_{H_1H_2}\big|_{x_F>0}}{(\sigma_{q\bar{q}}+\sigma_{gg})_{H_1'H_2}\big|_{x_F>0}}, \quad (6.8)$$

$$\sigma^{H_1H_2}_{q\bar{q}(gg)}\big|_{x_F>0} = \int_{4m_c^2}^{4m_D^2} dQ^2 \int_0^{1-\frac{Q^2}{s}} dx_F \sigma^{q\bar{q}\to c\bar{c}(gg\to c\bar{c})}(Q^2) \times \frac{x_1x_2}{Q^2(x_1+x_2)}F^{H_1H_2}_{q\bar{q}(gg)}, \quad (6.9)$$

where $2m_c = 3.0$ GeV and $2m_D = 3.74$ GeV; these are, respectively, the $c\bar{c}$ and open charm production thresholds, while the elementary cross sections $\sigma^{q\bar{q}\to c\bar{c}}$ and $\sigma^{gg\to c\bar{c}}$ are proportional to $\alpha_s(Q^2)$ and can be found, for example, in [57] (see (3), (4) in [57]).

Let us consider the "gluon evaporation" model without the gluon contribution $F^{H_1H_2}_{gg}$ for comparison. Obviously, it differs from the duality model only as it

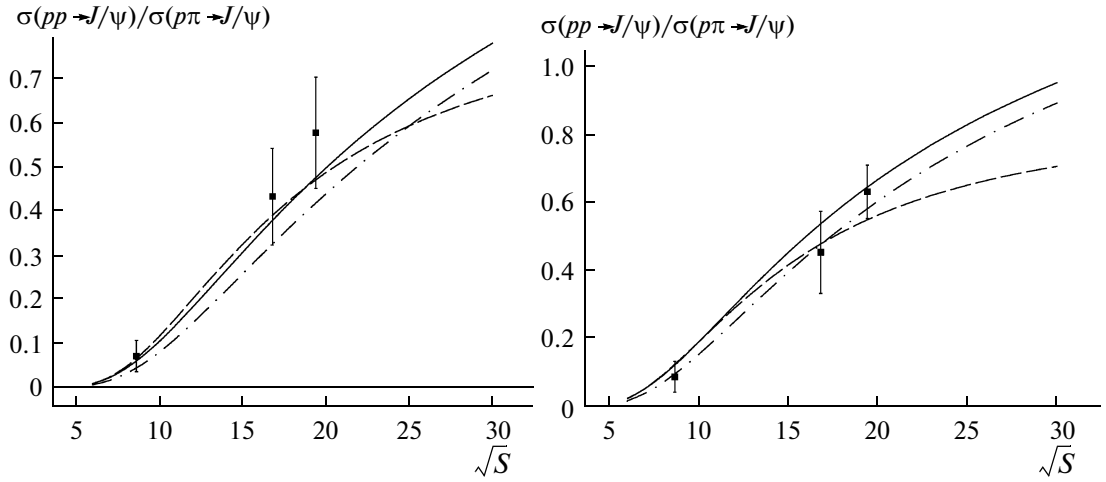

Fig. 6.1. Ratios of cross sections $\sigma_{pp}/\sigma_{\pi^{\mp}p}$ of J/ψ production calculated for two models in comparison with experimental data. Solid line corresponds to duality model (6.6), (6.7). Dashed line corresponds to "gluon evaporation" model (6.8), (6.9). Dash–dotted line corresponds to "gluon evaporation" model without account of gluon contribution. Parameterization GRV94 [39] for proton parton distributions and GRV [64] for pion parton distributions are used. Experimental data (points with error bars) are taken from [57] (Tables 2. and 3).

regards additional integration with respect to Q^2 with the weight $\sigma^{q\bar{q}\to c\bar{c}}(Q^2)$.

Let us first consider the ratios $\sigma_{pp}/\sigma_{\pi^{\pm}p}$. The results of application of the duality and "gluon evaporation" models in comparison with experimental data are shown in Fig. 6.1.

First of all, the following conclusion can be made from this figure: in the low-energy region near the first experimental point at $\sqrt{s} \simeq 8.7$ GeV the curves corresponding to the duality and "gluon evaporation" model, with and without the gluon contribution, are practically the same and well describe the experimental data. This is not surprising and agrees with the qualitative considerations: it was already discussed above that the gluon contributions should be suppressed in the low-energy region. At the same time, the results in the high energy region are somewhat surprising: even for very high energies (150 and 200 GeV) the gluon contributions are insignificant in the ratios $\sigma_{pp}/\sigma_{\pi^{\pm}p}$ and the curves with and without account of the gluon contributions $F_{gg}^{H_1H_2}$ well describe the available experimental data. Thus, in the case of a 150–200 GeV pion beam and the proton target it is necessary to considerably improve the quality of data on J/ψ production processes in order to feel the difference between the models with and without gluon contributions and evaluate the role of gluon–gluon fusion. It was already noted that experiments on investigation of processes (2.1), (6.2) and (2.2), (6.3) with the pion beam and the proton target are planned by the collaboration COMPASS [61]. In turn, experiments on processes (2.1), (6.2) and (2.2), (6.3) in proton–proton collisions with close kinematics are planned at the NICA accelerator complex.

A similar situation (insignificance of gluon contributions even for high energies) takes place also for the ratios $\sigma_{pA}/\sigma_{\pi^{\pm}A}$ with different target nuclei (see Fig. 6.2). Figure 6.2 shows the data with approximately similar $Z/A \simeq 0.4$. The curves corresponding to the model calculations were obtained with $Z/A = 0.4$ by neglecting nuclear effects,[23] so that the cross section per one nucleon has the form

$$\sigma_{hA}\big|_{h=\pi^{\pm},p} = \frac{Z}{A}\sigma_{hp} + \left(1-\frac{Z}{A}\right)\sigma_{hn}.$$

Let us consider the ratios $\sigma_{pp}/\sigma_{p\bar{p}}$ with the antiproton beam instead of the pion beam. The results are shown in Fig. 6.3. While in the low energy region the good agreement of the models with and without the gluon contribution, as well as the agreement of models with experimental data (as expected from the qualitative consideration) is observed, the situation in the high energy region turns out to be absolutely different. First of all, the conclusion can be made that the gluon contribution becomes essential in this kinematic region. The second unexpected conclusion is that the widely used "gluon evaporation" model works rather poorly in this case, the corresponding curve is noticeably lower than the experimental points (solid curve in Fig. 6.3). Note that this result is in strong contradiction with the statement made in [62] where the same experimental points were used.

[23] Usually [57] nuclear effects are accumulated in the factor A^{α}. However, for cross sections integrated with respect to x_F these factors almost do not differ from unity (see [57] and references therein.

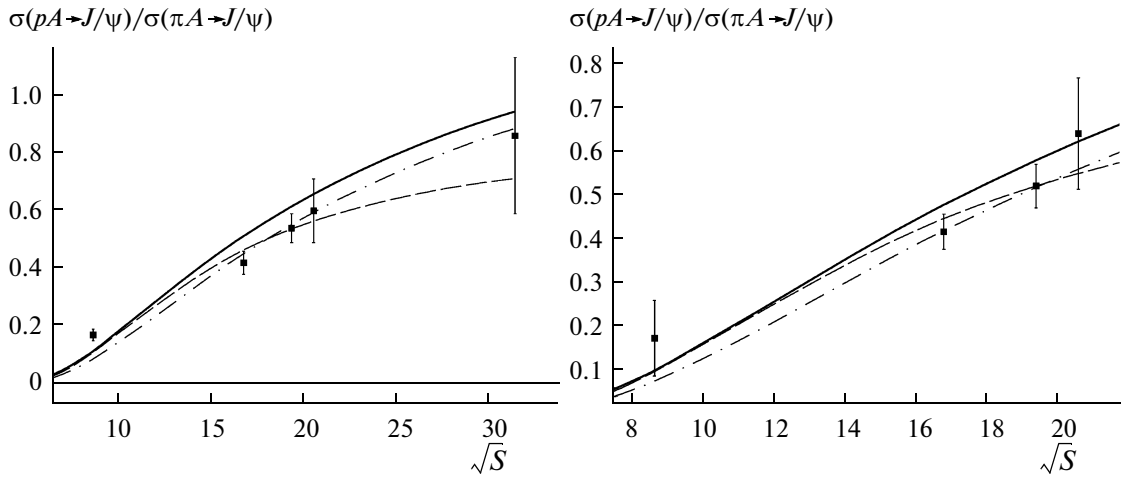

Fig. 6.2. Ratios of cross sections $\sigma_{pA}/\sigma_{\pi^{\mp}A}$ of J/ψ production for different nuclear targets ($Z/A \simeq 0.4$) calculated for two models in comparison with experimental data. Solid line corresponds to duality model (6.6), (6.7). Dashed line corresponds to "gluon evaporation" model (6.8), (6.9). Dash–dotted line corresponds to "gluon evaporation" model without account of gluon contribution. Parameterization GRV94 [39] for proton parton distributions and GRV [64] for pion parton distributions are used. Points with error bars show experimental data. First point W, $Z/A = 0.40$ [65]; second and third points Pt, $Z/A = 0.40$ [66]; fourth point C, $Z/A = 0.5$ [59]; fifth point Be, $Z/A = 0.44$ [67].

Indeed, the calculations in the framework of the "gluon evaporation" model presented in [62] (solid dashed line in Fig. 6.3) are in good agreement with the experimental points, which was commented as the strongest argument in favor of this model (see Fig. 6 in [62] and corresponding discussion). The reason of this discrepancy is the gluon[24] sector of the model, since the main difference of parameterization [63] used in [62] from modern parameterizations[25] used in our calculations is the values of gluon distributions. Of course, one should trust calculations with modern parameterizations, since the gluon's distribution function $G(x)$ in them is represented much better due to a great amount of new data that became available after [63] was published. The obtained results contradict experimental data, and thus, the conclusion can be made that for successful passing of the proposed test it is necessary to considerably modify the gluon sector of the "gluon evaporation" model. This test for high energy behavior should be passed by all existing models that pretend to reliably describe processes (6.2).

Thus, the duality and the "gluon evaporation" model were tested in different energy ranges. It was shown that the duality model (similar to the "gluon evaporation" model) works well in the low energy sector $s \leqslant 100$ GeV^2. In this region the curves obtained with and without account of the gluon contribution practically coincide and well describe the available data. Thus, this attractive from the theoretical point of view duality model can be reliably used (at least in the unpolarized case) in this kinematic region. This gives the unique capability of using J/ψ production processes together with Drell–Yan processes for finding parton distributions, which in turn allows one to considerably reduce statistical uncertainties for these distributions.

On the other hand, we encountered two rather surprising phenomena in the high energy region. The first one is related to pion–proton nuclear collisions for which the gluon contribution into the studied cross-section ratios seems insignificant even for a pion beam energy of 150–200 GeV. The second surprise is connected with antiproton–proton collisions. Here, on the one hand, the gluon contribution into the ratio $\sigma_{pp}/\sigma_{p\bar{p}}$ is quite essential in the high energy region, as expected. On the other hand, the description of this contribution in the framework of the most popular and widely used J/ψ production's "gluon evaporation" model is not consistent with experimental data. Thus, it seems that this model should be essentially modified (at least, as it regards the gluon sector of the model).

All results of tests definitely point to the fact that further theoretical and experimental effort is necessary for answering the existing questions. New information on the lepton pair's production in the region of J/ψ resonance both for high and low energies is required. This is especially related to polarized processes (2.2) and (6.3) for which any experimental data are still lacking. At the same time, the investigation of these

[24] This can be clearly seen from Fig. 6.3. Indeed, the curves corresponding to the "gluon evaporation" model without the gluon contribution practically coincide for the old and new parameterizations (thin dashed and solid lines in Fig. 6.3).

[25] Here, the result obtained using the popular widely used parameterization GRV98 [32] is presented. However, our calculations with other modern parameterizations yield the same picture (the results insignificantly differ from the corresponding results with the parameterization GRV98.

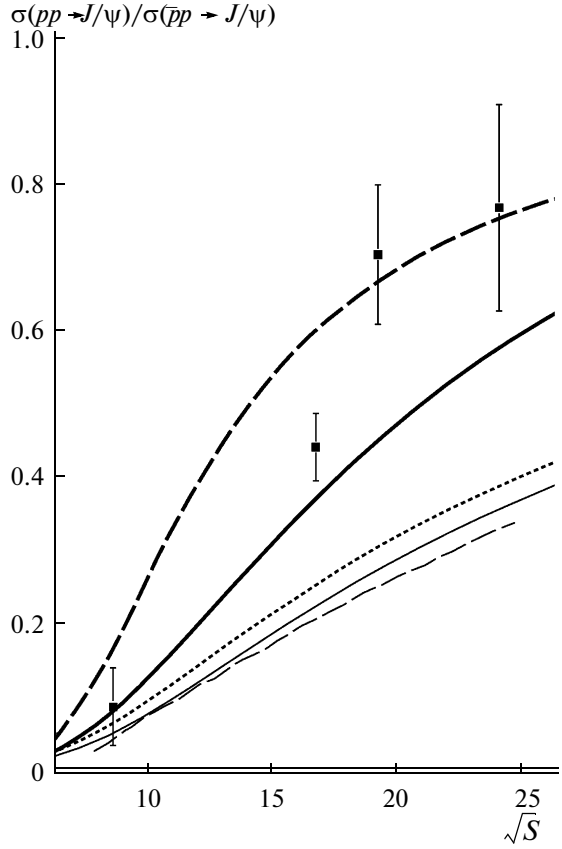

Fig. 6.3. Ratios of cross sections $\sigma_{pp}/\sigma_{p\bar{p}}$ of J/ψ production for proton target calculated for two models in comparison with experimental data. Experimental data are taken from [62] (data of collaborations NA3, WA39, and UA6), see Fig. 6 in [62]. Thick solid and dashed lines correspond to calculation using "gluon evaporation" model (with parameterizations GRV94 [32] and Duke–Owens [63], respectively). Thin solid and dashed lines correspond to calculations using "gluon evaporation" model without account of gluon contribution (with parameterizations GRV98 [32] and Duke–Owens [63], respectively). Dashed line corresponds to calculation using duality model with parameterization GRV98 [32].

processes (future experiments at COMPASS, NICA, RHIC, GSI, and J-PARC) should help us to finally find a number of poorly studied polarized parton distributions. In this case, the application of the duality model for processes (2.2) and (6.3) can considerably increase the accuracy of extraction of these distributions from data. In this regard, the precision verification of the duality model in future experiments for processes (2.1), (6.2) and (2.2), (6.3) becomes especially topical.

7. CONCLUSIONS

In conclusion let us discuss the problems and prospects of investigation of Drell–Yan processes.

From the considerations of practical expedience we did not discuss longitudinally polarized Drell–Yan processes, among which the most interesting ones, are processes with longitudinal polarization of both colliding hadrons. Indeed, at first glance it seems that the double-spin asymmetries corresponding to such processes, for example, in pp collisions (RHIC, NICA, COMPASS, and J-PARC),

$$A_{LL} = \frac{d\sigma_{\rightrightarrows} - d\sigma_{\leftrightarrows}}{d\sigma_{\rightrightarrows} + d\sigma_{\leftrightarrows}} \overset{LO}{=} \frac{\sum_q e_q^2[g_{1q}(x_1,Q^2)g_{1\bar{q}}(x_2,Q^2) + (q \leftrightarrow \bar{q})]}{\sum_q e_q^2[f_{1q}(x_1,Q^2)f_{1\bar{q}}(x_2,Q^2) + (q \leftrightarrow \bar{q})]},$$

can provide direct access to the poorly studied longitudinally polarized distributions of sea quarks $g_{1\bar{q}} \equiv \Delta\bar{q}$. However, similar to the case of the double-spin asymmetries A_{TT} (see Section 2) access to A_{LL} is extremely complicated due to high statistical uncertainties for these asymmetries (polarization factors for both hadrons in the error expression for low statistics of rare Drell–Yan events). At the same time, a good tool for investigation of longitudinally polarized (unlike transversely polarized) parton distributions are inclusive and semi-inclusive deep inelastic lepton scattering on nucleons (see, e.g., survey [55]); a great amount of precision data were obtained on these processes, and the data collecting continues presently at a high rate. Thus, the measurement of the double-spin asymmetries A_{LL} would hardly justify the colossal accelerator's time consumption necessary for observability. As it was discussed in detail above, the most reasonable (and necessary) is the investigation of unpolarized and single polarized Drell–Yan processes (2.1) and (2.2). At the same time, the measurements of very interesting (alternative access to transversity) double-spin asymmetries (2.10) in processes (2.3) could also be included in the physical programs of experiments on Drell–Yan processes (at present this possibility is studied in the framework of PAX and NICA projects), but only in the case of providing high level polarization and sufficiently large accelerator time.

It was already noted that the investigation of Drell–Yan processes with a valence antiquark in the initial state is extremely important. Moreover, processes involving antiprotons are especially important; they provide direct access to the distribution function of valence quarks in the proton without additional unknown variables, unlike, for example, the case of pion–proton collisions. At present, Drell–Yan processes with polarized antiprotons and protons are planned to be studied at the GSI accelerator complex (project PAX [52]). There exist a number of unsolved technical problems in the framework of the PAX project, the most important one is the creation of a sufficient polarization degree of the antiproton beam. In this regard, it seems reasonable to shift accents of the PAX physical program and make the investigation of unpolarized and singly-polarized Drell–Yan events

in antiproton–proton collisions the first priority task. On the other hand, in spite of the fact that in the Drell–Yan program of the collaboration COMPASS the first priority task is the investigation of Drell–Yan processes with pion participation, it would be highly desirable to include measurements with the antiproton beam into the Drell–Yan program at COMPASS. At present, this possibility is studied by the collaboration.

Drell–Yan processes with sea antiquark in the initial state are no less important since they provide access not only to valence, but also to sea distributions. It was demonstrated in this paper that the most promising are the corresponding studies in the collider mode (accelerator facilities RHIC and NICA). In this regard, promising is the fact that the physical programs of RHIC and NICA correspond to different kinematic regions, and in the case of their successful realization it would be possible to find the parton's distribution functions in the whole range of the Bjorken variable x.

It should be underlined once more that the studies in the region of J/ψ resonance are extremely important. If the hypothesis on duality of Drell–Yan and J/ψ production processes were proven, the unique chance of essential increase in the accuracy of extraction of unknown parton distributions would be obtained, which is especially important taking into account relatively low statistics of rare Drell–Yan processes.

REFERENCES

1. V. Barone, A. Drago, and P. G. Ratcliffe, Phys. Rep. **359**, 1 (2000); hep-ph/0104283.
2. A. V. Efremov et al., Phys. Lett. B **612**, 233 (2005).
3. J. C. Collins et al., Phys. Rev. D **73**, 014021 (2006).
4. M. Anselmino et al., Phys. Rev. D **75**, 054032 (2007).
5. A. Airapetian et al. (HERMES Collab.), Phys. Rev. Lett. **84**, 4047 (2000); Phys. Rev. D **64**, 097101 (2001); Phys. Lett. B **562**, 182 (2003); Phys. Rev. Lett. **94**, 012002 (2005).
6. E. S. Ageev et al. (COMPASS Collab.), Nucl. Phys. B **765**, 31 (2007).
7. V. A. Matveev, R. M. Muradian, and A. N. Tavkhelidze, Preprint OIYaI R2-4543 (Dubna, 1969); Preprint SLAC-TRANS-0098.
8. S. D. Drell and T. M. Yan, Preprint SLAC SLAC-PUB-0755 (1970); Phys. Rev. Lett. **25**, 316 (1970).
9. J. C. Collins, Phys. Lett. B **536**, 43 (2002).
10. J. Collins, "Rapidity Divergences and Valid Definitions of Parton Densities," in *Proc. of LIGHT CONE 2008*; arXiv:0808.2665v2 [hep-ph].
11. V. Barone, A. Prokudin, and B.-Q. Ma, Phys. Rev. D **78**, 045022 (2008).
12. H. Avakian, A. V. Efremov, P. Schweitzer, and F. Yuan, Phys. Rev. D **78**, 114024 (2008); S. Boffi, A. V. Efremov, B. Pasquini, and P. Schweitzer, Phys. Rev. D **79**, 094012 (2009).
13. A. N. Sissakian, O. Yu. Shevchenko, A. P. Nagaytsev, and O. N. Ivanov, Phys. Rev. D **72**, 054027 (2005).
14. A. Sissakian, O. Shevchenko, A. Nagaytsev, and O. Ivanov, Eur. Phys. J. C **59**, 659 (2009).
15. D. Boer, Phys. Rev. D **60**, 014012 (1999).
16. A. Bianconi and M. Radici, Phys. Rev. D **71**, 074014 (2005).
17. J. S. Conway et al., Phys. Rev. D **39**, 92 (1989).
18. S. Falciano et al. (NA10 Collab.), Z. Phys. C. **31**, 513 (1986); M. Guanziroli et al., Z. Phys. C **37**, 545 (1988).
19. A. Kotzinian and P. J. Mulders, Phys. Lett. B **406**, 373 (1997).
20. D. Boer, R. Jakob, and P. J. Mulders, Nucl. Phys. B **504**, 345 (1997).
21. D. Boer, R. Jakob, and P. J. Mulders, Phys. Lett. B **424**, 143 (1998).
22. D. Boer and P. J. Mulders, Phys. Rev. D **57**, 5780 (1998).
23. M. Anselmino, U. D'Alesio, and F. Murgia, Phys. Rev. D **67**, 074010 (2003).
24. M. Anselmino et al., Eur. Phys. J. A **39**, 89 (2009). Phys. Rev. D **79**, 054010 (2009).
25. A. Sissakian, O. Shevchenko, A. Nagaytsev, O. Denisov, and O. Ivanov, Eur. Phys. J. C **46**, 147 (2006).
26. J. C. Collins et al., Phys. Rev. D **73**, 094023 (2006).
27. T. Sjostrand et al., hep-ph/0308153.
28. M. Anselmino, V. Barone, A. Drago, and N. N. Nikolaev, Phys. Lett. B **594**, 97 (2004).
29. A. Bacchetta, M. Boglione, A. Henneman, and P. J. Mulders, Phys. Rev. Lett. **85**, 712 (2000); hep-ph/9912490.
30. J. Soffer, Phys. Rev. Lett. **74**, 1292 (1995).
31. M. Gluck, E. Reya, M. Stratmann, and W. Vogelsang, Phys. Rev. D **63**, 094005 (2001).
32. M. Gluck, E. Reya, and A. Vogt, Eur. Phys. J. C **5**, 461 (1998).
33. D. Hill et al. (RHIC Spin Collab.), Letter of Intent RHIC-SPIN-LOI-1991, updated 1993; G. Bunce et al., Particle World **3**, 1 (1992); K. Imai et al. (PHENIX/Spin Collab.), BNL-PROPOSAL-R5-ADD (1994); O. Martin, A. Schäfer, M. Stratmann, and W. Vogelsang, Phys. Rev. D **57**, 3084 (1998); Phys. Rev. D **60**, 117502 (1999).
34. J. Chiba et al., "Measurement of High-Mass Dimuon Production at the 50-GeV Proton Synchrotron," J-PARC Proposal, http://j-parc.jp/NuclPart/pac_0606/pdf/p04-Peng.pdf
35. M. Colantoni, Talk given at Transversity 2008 Workshop, May 28–31, 2008, Ferrara, Italy, http://www.fe.infn.it/transversity2008/.
36. A. Nagaitsev, "Spin Physics at NICA," Talk given on the NICA Round Table Discussion III (Dubna 2008), http://theor.jinr.ru/meetings/2008/roundtable/ .
37. A. Sissakian et al., "Design and Construction of Nuclotron-based Ion Collider facility (NICA)", Conceptual Design Report (Dubna, 2007); http://nuclserv.jinr.ru/nica_webpage/Nica_files/reports/CDR_07/CDR_NICA%20.html
38. A. N. Sissakian, A. S. Sorin, and V. D. Toneev, "QCD Matter: A Search for a Mixed Quark-Hadron Phase," nucl-th/0608032.

39. M. Gluck, E. Reya, and A. Vogt, Z. Phys. C **67**, 433 (1995).
40. M. Anselmino et al., Phys. Rev. D **72**, 094007 (2005).
41. W. Vogelsang and F. Yuan, Phys. Rev. D **72**, 054028 (2005).
42. A. Bacchetta, U. D'Alesio, M. Diehl, and C. A. Miller, arXiv:hep-ph/0410050.
43. V. Y. Alexakhin et al., Phys. Rev. Lett. **94**, 202002 (2005); hep-ex/0503002.
44. R. Seidl et al. (Belle Collab.), Phys. Rev. Lett. **96**, 232002 (2006).
45. O. Martin, A. Schäfer, M. Stratmann, and W. Vogelsang, Phys. Rev. D **57**, 3084 (1998).
46. P. V. Pobylitsa, hep-ph/0301236.
47. A. V. Efremov, K. Goeke, and P. V. Pobylitsa, Phys. Lett. B **488**, 182 (2000); hep-ph/0004196.
48. http://wwwasd.web.cern.ch/wwwasd/geant/.
49. A. Bianconi and M. Radici, Phys. Rev. D **73**, 034018 (2006); Phys. Rev. D **72**, 074013 (2005).
50. A. Bianconi, arXiv:0806.0946 [hep-ex].
51. N. C. R. Makins, GMC_trans Manual, HERMES Internal Report 2003, HERMES-03-060; G. Schnell, Talk at Workshop Transversity'07, ECT Trento, Italy, June 2007
52. V. Barone et al. (PAX Collab.), hep-ex/0505054.
53. M. Anselmino, V. Barone, A. Drago, and N. Nikolaev, Phys. Lett. B **594**, 97 (2004).
54. V. Barone, Z. Lu, and B. Ma, Eur. Phys. J. C **49**, 967 (2007).
55. A. Sissakian, O. Shevchenko, and O. Ivanov, Pis'ma Zh. Eksp. Teor. Fiz. **86**, 863 (2007) [JETP Lett. **86**, 751 (2007)].
56. E. Leader and E. Predazzi, *Introduction to Gauge Theories and the 'New Physics'* (Cambridge Univ., Cambridge, 1982).
57. R. Vogt, Phys. Rep. **310**, 197 (1999).
58. M. J. Corden et al. (WA39 Collab.), Phys. Lett. B **98**, 220 (1980).
59. K. J. Anderson et al., Phys. Rev. Lett. **42**, 944 (1979).
60. K. J. Anderson et al., Phys. Rev. Lett. **42**, 948 (1979).
61. P. Abbon et al. (COMPASS Collab.), Nucl. Instrum. Methods Phys. Res. A **577**, 455 (2007).
62. C. Morel et al. (UA6 Collab.), Phys. Lett. B **252**, 505 (1990).
63. D. W. Duke and J. F. Owens, Phys. Rev. D **30**, 49 (1984).
64. M. Gluck, E. Reya, and A. Vogt, Z. Phys. C **53**, 651 (1992).
65. M. J. Corden et al. (WA39 Collab.), Phys. Lett. B **96**, 411 (1980).
66. J. Badier et al. (NA3 Collab.), Z. Phys. C **20**, 101 (1983).
67. V. Abramov et al. (E672/706 Collab.), Preprint FERMILAB-PUB-91-062-E; Preprint IFVE-91-9 (March 1991).
68. M. Gluck, E. Reya, M. Stratmann, and W. Vogelsang, Phys. Rev. D **53**, 4775 (1996).